cy 1

AN INVESTIGATION OF BASE HEATING WITH A 5.47-PERCENT SATURN SA-1 BOOSTER MODEL AT MACH NUMBERS 0.8 AND 1.15

By

Joseph R. Parker, Jr. and T. J. Gillard
Rocket Test Facility
ARO, INC.

November 1961

ARNOLD ENGINEERING DEVELOPMENT CENTER
AIR FORCE SYSTEMS COMMAND
UNITED STATES AIR FORCE

NOTICES

AN INVESTIGATION OF BASE HEATING WITH A 5.47-PERCENT SATURN SA-1 BOOSTER MODEL AT MACH NUMBERS 0.8 AND 1.15

By

Joseph R. Parker, Jr. and T. J. Gillard

Rocket Test Facility
ARO, INC.,
a subsidiary of Sverdrup and Parcel, Inc.

November 1961

Program Structure 921E, Project 9018
ARO Project No. 114108

Contract No. AF 40(600)-800 S/A 24(61-73)

ABSTRACT

An investigation was conducted to determine the base recirculation characteristics of the simulated propellant pump turbine exhaust gases of a 5.47-percent scale model of the SA-1 Saturn afterbody. Gaseous hydrogen was used to simulate the combustible turbine exhaust gas of the full-scale missile. Base heating and pressure data were obtained at simulated flight trajectory conditions of Mach number 0.8 (16,000-ft altitude) and Mach number 1.15 (27,500-ft altitude) using several turbine exhaust duct configurations. In addition, the effect on base heating with one engine inoperative, of variation in turbine exhaust gas momentum, of finned-model operation, of variation in engine O/F ratio, and of variation in altitude was also investigated.

At both simulated flight trajectory conditions, the lowest base heating rates were obtained using a streamlined turbine exhaust duct configuration. The following conditions were found to reduce base heating, based on data obtained with the long turbine exhaust ducts: operation with one engine inoperative, increased turbine exhaust gas discharge momentum, and increased engine O/F ratio. With airflow over the model, heating rates to the flame shield (located between the four center engines) increased as altitude was increased from 15,000 to 27,500 ft. Without airflow, no further increase was noted at altitudes from 40,000 to 85,000 ft. Base heating rates obtained using the finned model were 40 percent higher than those obtained using the non-finned model.

CONTENTS

TABLES

ILLUSTRATIONS

NOMENCLATURE

A	Area, ft^2
C_P	Pressure coefficient
h	Simulated altitude, ft
M	Free-stream Mach number
MV/A	Turbine exhaust gas momentum/unit area, lb_f/ft^2
m	Calorimeter slug weight, lb
O/F	Ratio of engine oxidizer flow to fuel flow
p	Pressure, psia
q	Heat transfer rate, Btu/ft^2-sec
T	Temperature, °F
t	Time, sec

SUBSCRIPTS

B	Base
E	Heat transfer rate resulting from engine exhaust
FS	Flame shield
H	Heat transfer rate resulting from hydrogen burning
H_{ADJ}	Adjusted heat transfer rate due to hydrogen burning
HR	Heat ratio
s	Test section free stream
T	Adjusted total heat transfer rate
∞	Test section static

INTRODUCTION

The interaction of the external flow stream and the engine exhaust jets and the impingement of the exhaust jets upon each other produce a flow phenomenon which results in recirculation of hot, fuel-rich gases into the base of the SA-1 Saturn booster. These gases come from the main engine exhaust and from the propellant pump turbine exhaust and may combine with atmospheric air, ignite, and burn at the base. Such burning, with the attendant high heat release, may cause damage to vital engine controls and accessories. The arrangement of the four center engines produces a separate flow recirculation phenomena which can result in very severe base heating, especially at high altitudes, as explained in Refs. 1 and 2. Because the Saturn booster has a very complex engine cluster arrangement, the heating in the center of the inside cluster may be significant, even at low altitudes.

This report presents the results of tests conducted in the Rocket Test Facility (RTF), Arnold Engineering Development Center (AEDC), Air Force Systems Command (AFSC), with a 5.47-percent scale model of the Saturn SA-1 afterbody. The primary purpose of this investigation was to evaluate the effect on base heating of the discharge of combustible gases from the turbine exhausterators and several different overboard turbine exhaust duct configurations. In addition to the primary objective, base heating data were obtained with one engine inoperative, for a variation in turbine exhaust gas momentum, for a finned-model configuration, for a variation in engine O/F ratio, and at various altitudes. The investigation was conducted during the period February 15 through June 28, 1961, and was sponsored by the National Aeronautics and Space Administration.

APPARATUS

TEST ARTICLE

The 5.47-percent scale model of the SA-1 Saturn afterbody used in this investigation was constructed to match the diameter (13.92-in.) of existent mounting hardware (Figs. 1 and 2). Simulation of the aft shroud contours was provided from model station 0 forward to model station 9.2, a section which is equivalent to the aft-most 167.5-in. of the prototype

---

Manuscript released for publication October 1961.

booster. That portion of the model forward of model station 9.2 was cylindrical in cross section instead of having the scalloped cross section of the prototype booster caused by the eight propellant tanks. Minor external protuberances such as tie-down lugs, retro-rockets, and umbilical disconnects were not simulated on the model. Air scoops (Fig. 2a) were simulated because it was felt that these would have a direct influence on base heating.

Eight liquid oxygen, RP-1 fueled rocket engines (Fig. 3), each developing about 500-lb thrust, were used to simulate the prototype engines. Design data on the engines are presented in Table 1. Ignition was accomplished using a pyrophoric fuel, triethylaluminum. The engines were operated at a nominal chamber pressure of 500 psia and at nominal O/F ratios of 1.7 and 2.2.

The model engines were clustered, as shown in Fig. 2d, with the four inboard engines parallel to the model centerline and the four outboard engines fixed at a 6-deg outboard cant from the model centerline. The arrangement differed from that of the prototype engine mounting in which the four prototype inboard engines are fixed at a 3-deg outboard cant. This cant could not be duplicated on the model engines because of propellant and coolant line interference forward of the engine mounting plate.

The prototype propellant-pump turbine exhaust system was simulated by hydrogen discharged from exhausterators placed around each of the four outboard engines and from overboard ducts to each of the four inboard engines (Fig. 2). Details of the model exhausterator design and comparison with the prototype are presented in Fig. 4. Exact simulation of the turbine exhaust gas flow direction from the exhausterators could not be achieved because the model engine nozzle coolant jacket design did not conform to the external contours of the prototype engines.

Three overboard duct configurations were investigated; the details of each are shown in Fig. 5. The long overboard duct configuration was investigated first and most extensively. Comparison of the base heating rates obtained using this configuration with those obtained using the other duct configurations and from the configuration with stabilizing fins (Fig. 6) were then obtained.

INSTRUMENTATION

Design and fabrication of the model heat and flame shield (Figs. 1 and 2) and total heat transfer calorimetery followed closely the concepts proposed in Ref. 3. The shields were of a sandwich-type construction, as shown in

Fig. 7. The copper sheet was prepared by sandblasting and then plated with cobalt sulfide to give a black surface of high emissivity. This sheet was backed up by 0.38-in. thick insulation material to eliminate heat losses through the back side of the copper. The construction was completed with a solid steel backing plate for structural rigidity.

The calorimeters used to measure total (convective plus radiation) heat transfer were punched from copper sheet prepared in the same manner as the heat shield to give an identical surface. These slugs were inserted in holes cut from the copper heat shield and were cemented in place with a high temperature, low conductivity porcelain cement so that the slug was flush with the heat shield surface. Twenty-eight gage chromel-alumel thermocouple wires silver-soldered to the rear face of the slugs were passed through the insulation and backing plate and connected to a temperature recording device.

Heat and flame shield pressure measurements were obtained from static pressure orifices mounted flush on the shields. Location of all heat and flame shield instrumentation is shown in Fig. 8.

The calorimeter thermocouple millivolt outputs were recorded at 0.3-sec intervals on magnetic tape by a high speed digital recording system. Playback of this tape on an IBM-7070 computer gave a printed digital output of temperature variation with time. Millivolt outputs from transducers measuring base pressures, test cell total and static pressures, and test section free-stream pressure (p_s) were recorded at approximately 1.2-sec intervals and similarly converted to a tabulated digital printout.

Oxidizer and fuel tank pressures, injector pressures, and the individual engine chamber pressures were recorded on continuous direct-inking analog recorders. Individual oxidizer and fuel flows were measured with turbine-type flowmeters whose frequency outputs were recorded on an oscillograph. Engine coolant system pressures, temperatures, and flows were measured, and safety cut-outs were provided as required to determine and assure proper and safe operation.

Two 16-mm movie cameras were mounted on the perforated duct test section at the exit plane of the engine exhaust nozzles to record the ignition sequence, main stage lightoff, and burning pattern of the recirculated combustible gases.

A summary of model and test cell instrumentation showing the method and precision of measuring and recording data is given in Table 2.

INSTALLATION

The model and centerbody were cantilever-mounted from a spider arrangement in the forward portion of the test cell and extended aft through a 42-in.-diam bellmouth nozzle (Fig. 9). The model was enclosed in a perforated duct test section to permit a portion of the primary airflow to be bled into the surrounding low pressure region. The resulting flow expansion permitted the primary airflow to reach supersonic flow without an increase in test section area being necessary. Bleed suction was provided by the auxiliary bleed duct shown in Fig. 9. A 5-ft-diam duct with a conical inlet located at the exit of the perforated duct acted as a diffuser for the primary airflow. A 2-ft-diam duct was located concentrically in the 5-ft-diam ducting to capture the exhaust gases; this prevented mixing with the primary airflow and thus prevented thermal choking in the 5-ft-diam duct.

All the model instrumentation and control lines and the engine propellant and coolant supply, bleed, and return lines were run through the model and out the support spider and were then connected to facility plumbing and instrumentation in the plenum chamber. Mating lines, in turn, entered the plenum chamber through a pressure-tight porthole from the various facility propellant, coolant, and instrumentation systems (Ref. 4).

Hydrogen gas, which simulated the prototype turbine exhaust gases, was supplied from a common manifold having eight outlets; each outlet incorporated a 0.055-in.-diam orifice for flow regulation.

PROCEDURE

Airflow calibrations were performed, and the test section perforations were altered until a uniform axial flow field was obtained along the contoured model shroud. Thereafter, nozzle inlet total pressure and test section static pressure (p_∞) were set at values corresponding to the desired altitude and Mach number. Nozzle inlet total temperature was maintained at 100°F ± 5°F for all testing.

High altitude, Mach number zero runs were accomplished by closing the main airflow valves and exhausting the test cell to the desired pressure altitude prior to firing.

Prior to each test run, the heat and flame shields were blackened by a fuel-rich oxyacetylene torch to provide similar surface conditions for all runs.

When the desired tunnel conditions were established, the rocket firing sequence was initiated at a time designated T + O. A typical time history showing test cell and engine chamber pressure buildup is presented in Fig. 10.

Hydrogen was discharged from the exhausterators only, from the overboard ducts only, and from both simultaneously. A typical calorimeter temperature and heat transfer history is shown in Fig. 11. Engine-only data were obtained after steady-state engine operation had been established and before the hydrogen flow had been initiated. The flow rate of hydrogen gas is referred to in this report in terms of heat ratio, which is the ratio of the heat content of the discharged hydrogen gas to the equivalent heat content of the prototype missile turbine exhaust gases. Further definition and the methods of calculation are given in the appendix. When hydrogen gas flow was equivalent to a heat ratio of 1.0, the flow momentum per unit area from the overboard ducts was calculated to be approximately 38 percent of the prototype turbine exhaust momentum.

Increased momentum was obtained by decreasing the turbine exhaust duct exit area or by increasing the mass of the discharged gas by mixing hydrogen and nitrogen.

The exit total and static pressures and the temperature of the prototype turbine exhaust were not simulated.

RESULTS AND DISCUSSION

The 5.47-percent Saturn SA-1 booster model was tested at two points on the simulated flight trajectory primarily to determine the base heating rates which resulted when a simulated turbine exhaust gas was discharged from different turbine exhaust duct configurations. Test results are presented concerning:

- Comparison of maximum base heating rates for three overboard turbine exhaust duct configurations
- Distribution of heat flux over the model base
- Effect on base heating of operation with one engine inoperative
- Effect of stabilizing fins on base heating
- Effect of variations in O/F ratio on base heating
- Variation of flame shield heating rates with altitude

- Effect of variation in turbine exhaust gas momentum on base heating
- Base pressures

Total heat rate, as used in this report, is the sum of the heat transfer rates (radiation and convection) resulting from the engine exhaust gas recirculation to the base and from the hydrogen gas which recirculated and burned at the model base. The method used to obtain these values is presented in the appendix.

Attempts were made to set a hydrogen gas flow equivalent to a heat ratio of 1.0 (see appendix) for each test firing, but actual heat ratios varied between 0.95 and 1.09 during the primary investigation, and larger variations were tolerated during the secondary investigations (see Table 3). Therefore, to correct for these variations, indicated heat transfer rates resulting from hydrogen burning were adjusted to a heat ratio of 1.0 by dividing by the actual heat ratio for the particular firing. It is felt that use of these adjusted values of heat rates puts the comparison of configurations on a more equitable basis.

Before hydrogen was discharged simultaneously from the exhausterators and overboard turbine exhaust ducts, several firings were made with hydrogen flow from the exhausterators only. Base burning was not detected during any of these firings.

COMPARISON OF BASE HEATING RATES FOR THREE OVERBOARD TURBINE EXHAUST CONFIGURATIONS

In the case of the prototype booster the turbine exhaust gases are relatively cool (650°F) in comparison with the temperature of the engine exhaust jets (5,200°F). Therefore, little increase in base heating should occur, even if these gases do recirculate into the base, unless the gases when combined with atmospheric air ignite and burn in or very near the base. Because the gases are fuel rich, the possibility of ignition does exist, provided the proper conditions of mixture ratio and stay time are present. The most obvious solution to the base heating problem then is to minimize the amount of recirculated turbine exhaust gases because it is not possible to control either mixture ratio or stay time.

Three different overboard turbine exhaust duct configurations (Fig. 5) were tested at simulated flight trajectory conditions of Mach 0.8 (16,000 ft) and Mach 1.15 (27,500 ft) to determine the configuration for which the total heating rates were lowest. The results of these tests are presented in Fig. 12 as a comparison of the maximum total heating rates obtained.

The cross-hatched section of each bar represents the average engines-only heating rates, and the solid section represents heating rates caused by hydrogen burning. The total heating rates shown are the maximum obtained with each configuration; however, values higher than those shown could have been present at non-instrumented locations on the heat and flame shields.

Of the three test configurations, the streamlined turbine exhaust duct configuration resulted in the lowest total peak heating rates at both Mach 0.8 and 1.15. At Mach 0.8 no increase in heat flux from hydrogen burning occurred at either the heat or flame shields. It could not be determined whether this was the result of a lack of hydrogen recirculation into the base or of recirculation without ignition. At Mach 1.15 the hydrogen definitely recirculated and burned near the heat shield, as shown by the increase in heat shield heating rates (8 Btu/ft^2-sec) caused by hydrogen burning; burning did not occur at the flame shield.

The most severe base heating occurred with the short overboard duct configuration; peak total base heating rates of 52.5 and 36.0 Btu/ft^2-sec at Mach 0.8 and 1.15, respectively, were produced.

The two extremes in heating rates were caused by the different amounts of hydrogen being drawn into the base. Thus the short ducts with the larger frontal area produced a larger and more turbulent wake than the airfoil-shaped streamlined ducts and, consequently, entrained a greater quantity of the discharged hydrogen, which was subsequently drawn into the model base to form a combustible hydrogen-air mixture. This larger quantity of hydrogen produced a larger heat release when the hydrogen-air mixture was ignited; the data show that the increase was approximately 60 percent at Mach 1.15.

The effect of the duct trailing wake was investigated further during two firings of the long overboard duct configuration made at the same simulated trajectory conditions; in one case the long ducts were mounted on airfoil-shaped brackets; in the other case they were mounted on structural (high blockage) brackets (Fig. 5). As shown in Fig. 12, the base total heating rates were reduced approximately 35 percent when the airfoil-shaped brackets were used.

DISTRIBUTION OF HEAT FLUX OVER MODEL BASE

To give a complete distribution picture, the total heating rates from individual calorimeters are shown in Fig. 13 for each turbine exhaust duct configuration and Mach number. At Mach 0.8 (Fig. 13a) when hydrogen

was discharged from the long and short overboard ducts, the highest total base heating rates were measured in the region located between the inboard and outboard engines; thus, the greatest concentration of hydrogen occurred in this region. Hydrogen discharged from the streamlined ducts did not burn, and consequently, a low, uniform heat flux distribution was obtained with this configuration.

At Mach 1.15 the heat flux distribution obtained when hydrogen was discharged from the short and streamlined ducts was similar to that obtained at Mach 0.8 (Fig. 13b). A somewhat different distribution was obtained with the long ducts. In this case, when the long ducts were mounted on the high blockage brackets, the highest heating rates were measured in the base region located between the inboard and outboard engines adjacent to the ducts. When the airfoil-shaped brackets were used, a reduction in heating rates occurred in this region, and the peak heating region was shifted to a location between the outboard engine and the model skirt.

Thus, based on total heat transfer rates, the most uniform base heat flux distribution was obtained with the streamlined ducts and the most nonuniform with the short ducts.

EFFECT ON BASE HEATING OF OPERATION WITH ONE ENGINE INOPERATIVE

Since the Saturn booster is capable of operation with one of the eight engines inoperative, it was desired to determine what changes would occur in the base heating rates in such a case. The condition was investigated with the No. 8 engine inoperative (propellant lines capped) because it was believed that a failure on an inboard engine would produce the most adverse effect on base heating. (Hydrogen was discharged from the long overboard ducts and exhausterators for all firings.)

Flame Shield

When the Saturn ring-cluster nozzle arrangement (center four engines) is operated in the lower altitude region with all engines operating, the jets do not impinge, and therefore, an aspirating effect is produced which pulls hot gases from the model base region into the area between the ring-cluster jets. This flow characteristic was confirmed by the increase in flame shield heating rates which occurred when hydrogen gas was discharged from the overboard ducts only. (Because the hydrogen originated outside the center area, aspiration had to occur for the hydrogen to be drawn into the center area.) However, when one of the ring-cluster engines is inoperative,

the center region is not enclosed, and much of the aspirating effect is lost, as indicated by the increase in the ratio of flame shield to base pressure (p_{FS}/p_B) shown below:

	p_{FS}/p_B	
Configuration	M = 0.8	M = 1.15
Eight Engines	0.72	0.90
Seven Engines	1.00	Not obtained

It is concluded that the major effects on flame shield heating of seven-engine operation are: (1) the decrease in aspiration which reduces the amount of hot gases (combustible or not) drawn into the center region, (2) the reduction of the radiation heat source by 25 percent, and (3) the decrease in back flow of hot gases from the exhaust jets into the center region as compared with that which probably occurs with eight-engine operation (even with aspiration).

At the higher altitude (Mach 1.15) the exhaust jets were larger, and the jet boundaries of the center four engines began to impinge; however, during eight-engine operation, the pressure ratio (shown above) indicates that some aspiration still existed. Apparently, however, it was not great enough to draw hydrogen into the center area because no hydrogen burned during eight-engine operation. During seven-engine operation hydrogen burned in the center region, and heat flux increased by 3.5 Btu/ft^2-sec, as shown in Fig. 14a. Flame shield pressures were not obtained during the seven-engine runs made at Mach 1.15.

Heat Shield

In general, base heat flux decreased when the No. 8 engine was inoperative (Fig. 14b). However, at Mach 0.8 base burning was apparently marginal; one of the two seven-engine firings resulted in heating rates slightly higher than those obtained for the eight-engine firing, and the other produced considerably lower heating rates, although trajectory conditions for these two firings were almost identical. At Mach 1.15, operation with one engine inoperative resulted in a large reduction in base heating rates, especially in the region located between the inboard and outboard engines (Fig. 14b).

EFFECT OF STABILIZING FINS ON BASE HEATING

Four stabilizing fins were installed on the model afterbody as shown in Fig. 6, and two firings were made at Mach 0.8 with hydrogen discharged from the long overboard ducts and exhausterator to obtain base heating data for comparison with data obtained from the non-finned configuration. The results are presented in Fig. 15. The change in the base flow pattern produced by the addition of the fins caused a 40-percent increase in average base heat flux. The fins altered the external flow field locally and created a large turbulent wake upstream of the model skirt trailing edge. This effect is evident from an examination of the base pressure ratios, p_B/p_∞, for the two configurations (see section on Base Pressure). Prior to engine ignition at Mach 0.8 external flow, the ratio was 1.07; after the addition of fins, the ratio decreased to 0.75. Effectively then, the fins induced a lower base pressure which either caused a larger quantity of hydrogen to be drawn into the base region or altered the hydrogen-air ratio in the base region or both. Either could cause more severe base burning.

EFFECT OF O/F RATIO ON BASE HEATING

Unless otherwise noted all data previously presented were obtained at a nominal O/F ratio of 1.7. To determine the effect of O/F ratio on base heating, additional firings were made at a nominal O/F ratio of 2.2. These data are presented in Figs. 16a, b, and c for the three basic turbine exhaust duct configurations. The comparison is presented primarily to show the trend in heating rates produced by variations in O/F ratio. Adjustments have not been made for variations in Mach number, altitude, hydrogen pressure, chamber pressure, exhaust flame temperature, and exhaust gas total weight flow, all of which could alter the magnitude of the heating rates shown.

Total heating rates measured on the flame shield (Fig. 16e) indicate that operation at the higher O/F ratio decreased hydrogen burning in the center region when the long and short duct configurations were used but increased burning when the streamlined ducts were used (Fig. 16f). The average flame shield heating rates resulting from engines-only operation remained fairly constant in spite of variations in O/F ratio.

Base total heating rates decreased, in general, when O/F ratio was increased from 1.7 to 2.2. (The exception was the case of the streamlined duct configuration.) The lower heating rates at the higher O/F ratio were assumed to be the result of a lower heat release from hydrogen burning in the base. No significant difference in base heating rates was observed for engines-only operation.

When the streamlined ducts were tested at Mach 0.8 and an O/F ratio of 1.7, no hydrogen burning occurred; however, with an O/F ratio of 2.24 the hydrogen definitely burned. It should be noted that only one firing was made with the streamlined ducts at the high O/F ratio and that during this test only three base calorimeters were operative (Fig. 16c).

Heat flux distribution over the base was essentially the same at O/F ratios of 1.7 and 2.2 for the short and long duct configurations. The distribution could not be determined for the streamlined ducts at an O/F ratio 2.2 because of the limited calorimeter instrumentation.

VARIATION IN FLAME SHIELD HEATING RATES WITH ALTITUDE

When the ring-cluster nozzle arrangement of the four inboard engines is operated in the lower altitude regions, the non-interfering jets produce an aspirating effect which, by pulling hot gases from the base region into the center of the cluster, can produce heating on the flame shield. The variation of the heat flux in the center of the inboard engine cluster is presented in Fig. 17 as a function of flame shield to base pressure ratio. Data obtained at low altitudes are shown for the conditions non-burning and burning. Because the hydrogen which burned in this region originated outside the region, the flow characteristic had to be that of aspiration to influence the heat flux to the flame shield.

At a pressure ratio of one it was assumed that no flow existed through the center area in either direction; at pressure ratios greater than one, gas was ejected from the jet boundaries into the center region and then ejected at a 90-deg angle to this rearward flow through the four triangular openings between the nozzle lips and the point of initial jet impingement (Fig. 17). The resulting heat flux to the flame shield appeared from the data to reach a maximum value which was not exceeded in spite of any further increase in the flame shield to base pressure ratio.

The flame shield calorimeter was located off-center and thus did not measure the maximum heat transfer rate which occurred at the center of the flame shield. If a measurement of maximum heating rates had been possible, the level of the curve in Fig. 17 would be higher, but the trend would be unaltered.

EFFECT OF VARIATION OF TURBINE EXHAUST GAS MOMENTUM ON BASE HEATING

The rate of hydrogen discharge from the turbine exhaust ducts simulated the heat content available from the turbine exhaust gases of the

full-scale system (for HR = 1.0). However, momentum simulation is also important because momentum determines the distance from the base the gases will travel before they mix with the external airstream. If this distance is small, as it would be with a low discharge momentum, most of the discharged gases can be drawn into the base region; if a high discharge momentum is used, the distance can be large and can result in little or no recirculation. This effect was investigated during several firings which were made with varying values of hydrogen gas discharge momentum. (Hydrogen was discharged from the overboard ducts only.)

Two methods of varying MV/A were used. The first method consisted of changing the exit area of the hydrogen ducts and discharging pure hydrogen. Values of MV/A in the range of 36 to 244 percent of the full-scale exhaust duct MV/A (965 lb_f/ft^2) were obtained. The second method utilized a constant duct exit area and varied MV/A by changing the mass of the discharged gas. This was done by mixing a heavier gas (nitrogen) with the hydrogen gas (flow orifices were sized to discharge the same quantity of hydrogen as in the first method). Two mixtures were used, one with 60-percent hydrogen and 40-percent nitrogen, the other with 20-percent hydrogen and 80-percent nitrogen by volume. The resulting values of MV/A ranged from 51 percent to 165 percent of full-scale MV/A.

Data from firings made using both methods of MV/A simulation are presented in Fig. 18. The heat transfer rates shown represent the maximum change in base heating rates attributed to the pure hydrogen or the hydrogen-nitrogen mixtures and therefore, do not reflect engines-only heating rates.

The curve obtained when MV/A was increased by decreasing the exit area of the ducts shows that base heating rates decreased from a maximum value of 37.5 Btu/ft^2-sec at 38 percent of full-scale MV/A to 17.5 Btu/ft^2-sec at 120 percent of full-scale MV/A. Between 120 and 244 percent of full-scale MV/A, no heat flux from hydrogen burning was measured, an indication that the increased discharge momentum carried the hydrogen far enough into the external airstream to prevent recirculation. Between 36 and 120 percent of full-scale MV/A the duct was not choked, and the exit velocity increased as the duct exit area was decreased. When MV/A was greater than 180 percent of the full-scale value, the duct exit was choked, and no further increase in velocity occurred.

When the hydrogen-nitrogen mixture was used to change MV/A, the same trend in base heating rates was obtained that resulted from variation in the duct area. However, the base heating rates were much lower for the

mixtures (Fig. 18) than for pure hydrogen within the same MV/A range in spite of the almost equal available heat content. It is assumed, then, that the nitrogen in the 60-percent hydrogen - 40-percent nitrogen mixture acted as a heat sink or shielded the hydrogen and reduced the degree of base burning. The 20-percent hydrogen - 80-percent nitrogen mixture was within the non-flammable limits (Ref. 5) and therefore did not ignite. Thus the negative heat flux change measured shows that the mixture was recirculated and provided a cooling effect in the base.

BASE AND FLAME SHIELD PRESSURE

Base pressure data presented in this report were obtained from an arithmetical average of the seven base pressure taps located as shown in Fig. 8. Flame shield pressure data were similarly obtained using the three flame shield pressure taps. No trend in pressure could be detected over either the base or the flame shield during any individual run. In general, the variation in individual base pressures was within ±5 percent of the average base pressure, and the variation in individual flame shield pressures was within ±1 percent of the average pressure.

The variation with Mach number of base pressure coefficient and of base to free-stream pressure ratio is shown in Figs. 19 and 20, respectively. With no base burning, as when no hydrogen was emitted or when hydrogen was emitted from the exhausterators only (Figs. 19a and 20a), both the base pressure coefficient and the pressure ratio decreased when Mach number was increased from 0.8 to 1.15. Thus the absolute base pressure decreased at a more rapid rate than did free-stream static pressure. This condition should be expected, however, because the higher velocity external airstream at Mach 1.15 would tend to exert a stronger pumping action at the base of the model.

When base burning occurred, the effect was an increase in the absolute base presure, as shown by Figs. 19b and 20b. As stated previously, no base burning occurred when the streamlined ducts were used at Mach 0.8. The figures show base pressure coefficient and pressure ratio values for this configuration and condition to be in good agreement with the no-base burning condition. At Mach 1.15, however, some burning was obtained, and the result is a net positive slope to the lines connecting Mach 0.8 and 1.15 data (Figs. 19b and 20b). Similar trends are shown for data obtained with the long and short overboard ducts. The differences in magnitude of the base pressure coefficient and the pressure ratio between configurations was the result, in part, of the degree of base burning which resulted and, in part, of the change in flow field at the model base created by the different duct shapes.

The effect of changes in the degree of base burning or of change in overboard duct configuration on flame shield pressures could not be detected. All flame shield pressure coefficient data fell within the envelope shown in Fig. 21a. Of interest, however, is the increased slope of the flame shield pressure coefficient data over the slope shown for base pressure coefficient (Fig. 19b) with increasing Mach number. This change is attributed to the fact that, as Mach number was increased from 0.8 to 1.15, free-stream pressure was decreased about 35 percent to maintain missile trajectory conditions. The slight spreading of the engine exhausts jets which resulted effectively decreased the vent area between the adjacent inboard engines. The net effect was that only a 26-percent decrease in flame shield pressure occurred as Mach number was increased, and the result is the steep positive slope of the flame shield pressure coefficient data (Fig. 19b).

The variation with Mach number of the ratios of flame shield to base pressure and flame shield to free-stream pressure is shown in Fig. 21b. At the lower Mach number condition, flame shield pressure was about 71 percent of free-stream pressure and 74 percent of base pressure. At Mach 1.15, flame shield pressure was about 80 percent of free-stream pressure (which reflects the approximately 9-percent decrease in pressure mentioned in the previous paragraph) and about 88 percent of base pressure.

When only seven of the eight engines were operated, a considerable decrease in base pressure parameters resulted (Fig. 22). This increase in base area purge was indicated by the base static pressure taps located opposite the non-burning engine (Fig. 8). In theory, base pressure in the region of the non-burning engine was even lower than that measured in the region of the static taps, because, as was pointed out earlier, a general decrease in heat flux was indicated when this configuration was used.

The negative slope of base pressure ratio data with increasing Mach number during operation with seven engines indicated that base pressure decreased at a faster rate than did free-stream pressure. The slope, however, is almost identical with that shown for the eight-engine, no base burning condition (Fig. 20a). Thus, the negative slope shown for seven-engine operation was the result of the increase in base purge caused by the higher velocity external airstream; increasing Mach number had no effect on the amount of base purge provided when the engine was not firing.

Data were obtained at Mach number 0.8 with eight engines operating and with the stabilizing fins (Fig. 6) installed to evaluate the effect of the fins on base heating and pressure. Base heating increased 40 percent when the fins were installed over the rate obtained without fins. Thus, it

might be concluded that the base pressure coefficient would be positive and that the base pressure ratio would be greater than 1.0 (Figs. 19b and 20b). This was not the case, however, as shown in Figs. 22a and 22b. Operation with the stabilizing fins installed increased the base purge, apparently because of the local acceleration of the external airstream as it flowed around and past the fins. The result was a 17-percent decrease in base pressure from that obtained without the fins installed.

SUMMARY OF RESULTS

The results obtained during the investigation of base heating with a 5.47-percent Saturn SA-1 booster model are summarized as follows:

1. Based on peak total base heat transfer rates, the most effective configuration for the overboard discharge of simulated turbine exhaust gases (hydrogen) was the streamlined turbine exhaust duct configuration. Peak total base heating rates were 10.0 and 15.0 Btu/ft^2-sec at Mach 0.8 and 1.15, respectively.

   Hydrogen discharge from the long turbine exhaust ducts resulted in peak total base heating rates of 26.5 and 33.8 Btu/ft^2-sec at Mach 0.8 and 1.15, respectively. Modification of the attachment brackets for the long ducts reduced the peak to 22.0 Btu/ft^2-sec at Mach 1.15.

   Hydrogen discharge from the short turbine exhaust ducts resulted in the most severe base heating at both Mach numbers; peaks were 52.5 and 36.0 Btu/ft^2-sec at Mach 0.8 and 1.15, respectively.

2. The region on the model base which indicated the highest heat transfer rate usually was located between the inboard and outboard engines.

3. During firings with one engine intentionally inoperative, the flame shield and base heat transfer rates were reduced; however, base burning appeared to be marginal for this configuration because one firing at Mach 0.8 resulted in base heating rates slightly greater than those obtained during operation with all eight engines.

4. Operation with the stabilizing fins installed on the model afterbody resulted in a 40-percent increase in average base heating rates above that of the non-finned configuration.

5. The major effect on base and flame shield heating of an increase in the nominal O/F ratio from 1.7 to 2.2 was to decrease hydrogen

burning in the case of the long and short duct configurations. However, the streamlined ducts did not follow this trend and indicated increased burning at both the base and flame shield.

6. Flame shield heat transfer rates increased rapidly when altitude was increased from 15,000 to 40,000 ft. Between 40,000 and 85,000-ft altitude (without external airflow) the heating rate was essentially constant.

7. Increasing the turbine exhaust gas momentum per unit area from 36 to 120 percent of the full-scale value resulted in decreasing base burning during the discharge of pure hydrogen and a hydrogen-nitrogen mixture. Base burning did not occur when the percentage of full-scale momentum per unit area was greater than 180 percent.

8. When hydrogen was discharged from the exhausterators only there was no measurable increase in base heating above that obtained from operation without hydrogen flow.

9. With no base burning, base pressure ratio decreased approximately 13 percent as Mach number was increased from 0.8 to 1.5 because of the increase in base pumping action created by the high velocity external airstream. When base burning did occur, base pressure ratio increased about 1 percent over the same Mach number range.

10. Flame shield pressure coefficient increased from -0.58 at Mach 0.8 to -0.23 at Mach 1.15. No influence of degree of base burning or of overboard duct configuration on flame shield pressures could be detected.

REFERENCES

1. Goethert, B. H. "Base Flow Characteristics of Missiles with Cluster Rocket Exhaust." Institute of Aerospace Sciences Paper No. 60-89, July 1960.

2. Goethert, B. H. "Base Heating Problems of Missiles and Space Vehicles." American Rocket Society Paper No. 1666-61, March 1961.

3. Westkaemper, J. C. "An Analysis of Slug-Type Calorimeters for Measuring Heat Transfer from Exhaust Gases." AEDC-TN-60-202, November 1960.

4. Test Facilities Handbook, (3rd Edition). "Rocket Test Facility, Vol. 2." Arnold Engineering Development Center, January 1961.

5. Drell, Isadore L. and Belles, Frank E. "Survey of Hydrogen Combustion Properties." NASA Report 1383, 1958.

APPENDIX

METHODS OF CALCULATION

HEAT TRANSFER

Total heat transfer, q_T, was computed for each calorimeter by obtaining the indicated calorimeter temperature rise over each 0.6-sec interval and using:

$$q_T = \frac{C_P m}{A} \left(\frac{dT}{dt}\right)$$

where q_T = Total heat flux, Btu/ft^2-sec

C_P = Specific heat of copper, Btu/lb-°F

m = Calorimeter slug weight, lb

A = Calorimeter slug exposed surface area, ft^2

$\frac{dT}{dt}$ = Temperature derivative with respect to time, °F/sec

BASE PRESSURE

Base pressure (p_B) data presented in this report were obtained by averaging the values from the seven static pressure taps located on the base. Flame shield pressure (p_S) data were obtained by averaging the values from the three static pressure taps located on the flame shield. Base and flame shield pressure coefficients are defined as

$$C_{P_X} = (p_X - p_\infty)/q_\infty$$

where p_X refers to either p_B or p_{FS}, and

$$q_\infty = 0.7\, p_\infty (m_\infty)^2$$

HEAT RATIO

Gaseous hydrogen was used to simulate the combustible turbine exhaust gases of the prototype system. Hydrogen was selected because of its wide flammability limits (4 to 74-percent hydrogen to air, by volume - Ref. 3) and was discharged at a rate which simulated the heat content that would be available (equivalent heat content):

1. If the turbine exhaust gases discharged from the model were of the same chemical composition as those of the prototype, and

2. If these gases were discharged from the model in the same proportion to model engine total propellant flow as the gases from the prototype, and
3. If a combustion efficiency of 100 percent were assumed for burning of the turbine exhaust gases.

Based on these assumptions, the turbine exhaust flows in this investigation were referred to in terms of heat ratio calculated as follows:

Given:
1. Total prototype propellant flow = 643 lb/sec/engine
2. Total prototype turbine exhaust gas flow = 13.25 lb/sec/engine
3. 57 percent of prototype turbine exhaust gas flow is unburned RP-1 with a heating value = 18,600 Btu/lb
4. Total model propellant flow = 2.22 lb/sec/engine
5. Lower heating value of gaseous hydrogen = 51,600 Btu/lb

Therefore, the ratio of prototype total propellant flow to combustible turbine exhaust gas flow = $\frac{643}{13.25 \times .57} = 85.1$.

To maintain the model flow ratio at this value would require 2.22/85.1 = 0.0261 lb/sec of unburned RP-1, with an available heat rate of 0.0261 x 18,600 = 485 Btu/sec. To obtain this heat rate with hydrogen gas, a flow of 485/51,600 = 0.0094 lb/sec would be required. Heat ratio was then defined as the actual hydrogen flow rate during each particular run divided by 0.0094. These values are tabulated for each test run in Table 3.

DETERMINATION OF HEAT RATES

Total heat rates, as referred to in the text, were defined as the sum of the convective and radiant heat rates resulting from: (1) engine exhaust gas recirculation and (2) hydrogen gas recirculation and burning at the model base and flame shield. The method used to obtain these values may be illustrated by the figure on the following page.

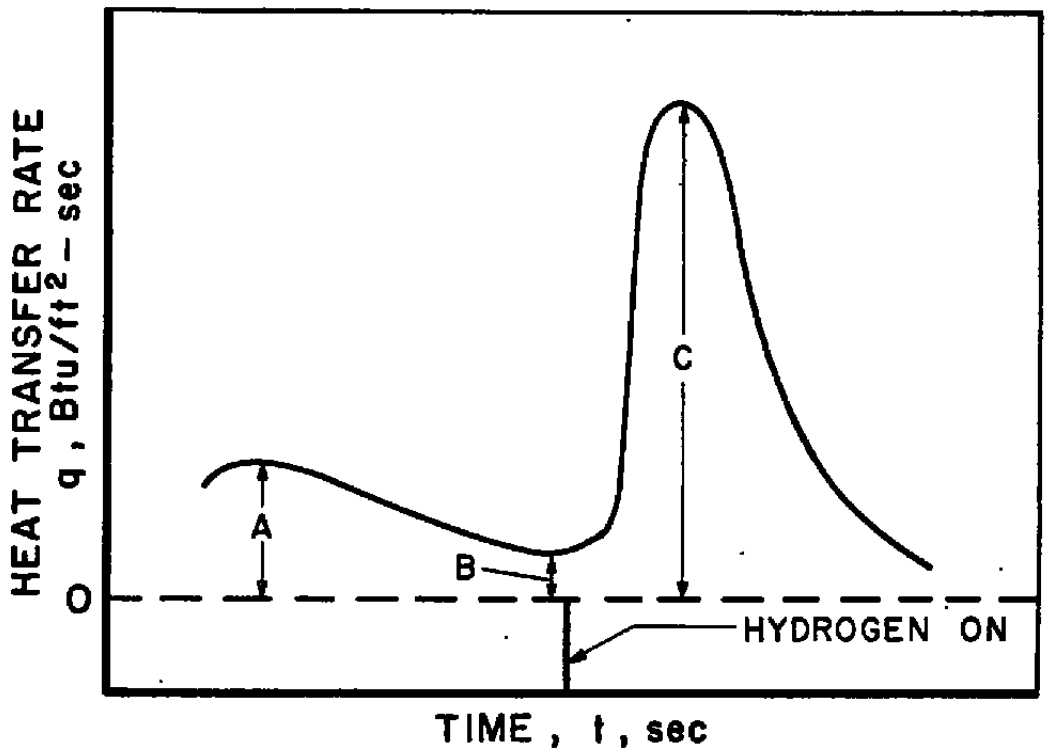

From each calorimeter heat transfer-time history the following heat transfer rates were obtained:

Heat rate resulting from engine exhaust gas recirculation, $q_E = A$

Heat rate resulting from hydrogen burning, $q_H = C - B$

The heat rate attributed to hydrogen burning, q_H, was assumed to be a direct function of heat ratio, which could not be maintained constant for all firings (Table 3). Therefore, to permit a direct comparison of heat rates for the different turbine exhaust configurations, the heat rate resulting from hydrogen burning, q_H was adjusted to a heat ratio (H. R.) of 1.0 by:

$$q_{H_{ADJ}} = \frac{q_H}{H.\ R.} = \frac{C - B}{H.\ R.}$$

The total heat rate was then defined as:

$$q_T = A + \frac{C - B}{H.\ R.}$$

The value of heat rate attributed to engine exhaust gas recirculation for each calorimeter was obtained by averaging q_E for all tests made with a given turbine exhaust configuration, and this value is presented as the cross-hatched portion of the bars on Fig. 12.

TABLE 1

ROCKET ENGINE DESIGN DATA

	Model	Prototype
Nozzle shape	Contoured	Contoured
Nozzle throat diam, in.	0.90	16.5
Nozzle exit diam, in.	2.50	46.74
Nozzle area ratio	7.72	8.0
LO_2 flow, lb/sec/engine	1.5 lb/sec	435
RP-1 flow, lb/sec/engine	0.7 lb/sec	190
Chamber pressure, psia	500 psia	575 ± 5
Coolant (water) flow rate, lb/sec	3 lb/sec nom.	None

TABLE 2

INSTRUMENTATION SUMMARY

Parameter	Method of Measurement	Method of Recording	Range	Response Time, millisec	Max Deviation, ± Percent of Full Scale
Calorimeter Temperature	C/A Thermocouple	Magnetic Tape	0-1800 °F	1.0	1.0
Base Pressure	Strain-Gage Transducer	Magnetic Tape	0-10 psia	1.0	0.75
Base Pressure	Strain-Gage Transducer	Oscillograph	0-10 psia	5.0	2.5
Free-Stream Pressure	Strain-Gage Transducer	Magnetic Tape	0-15 psia	1.0	0.75
Test Cell Total Pressure	Strain-Gage Transducer	Magnetic Tape	±15 psid	1.0	1.0
Combustion Chamber Pressure	Strain-Gage Transducer	Continuous Inking Recorder	0-1000 psig	500	2.0
Injector Pressure	Strain-Gage Transducer	Continuous Inking Recorder	0-1000 psig	500	2.0
Propellant Flows	Turbine-Type Flowmeter	Oscillograph	0-1.5 lb/sec	5.0	0.5

TABLE 3

SUMMARY OF CONDITIONS FOR INDIVIDUAL TEST FIRINGS

Run No.	Turbine Exhaust Duct Configuration	Mach No.	Altitude, ft	Heat Ratio	O/F Ratio	Remarks
46-2***	1*	1.17	27,500	1.092	1.63	Airfoil Bracket
46-4***	1	1.16	27,500	.963	1.68	Structural Bracket
46-6***	1	0.87	17,500	.984	1.66	
46-8***	1	0.86	17,400	.950	1.65	
61-2	1	0.73	14,000	.872	1.68	Fins
61-4	1	0.74	14,000	.895	1.70	Fins
66-4	1	0.97	23,000	.875	1.69	Engine Out
66-6	1	1.01	23,500	.857	1.80	Engine Out
66-8	1	0.77	15,500	.874	1.69	Engine Out
66-10	1	0.81	17,500	.953	2.07	Engine Out
67-2	1	0.77	15,000	.890	1.61	Engine Out
67-4	1	0.82	16,600	.940	2.09	Engine Out
68-2	1	0.81	16,000	.979	2.28	
68-4	1	0.81	16,500	1.025	2.29	
70-6	1	0.85	17,500	**	2.29	
81-6	1	1.00	23,500	.990	2.16	
42-2***	2	1.17	27,700	.991	1.96	
42-4***	2	1.17	28,000	1.014	1.77	
44-2***	2	0.83	16,500	.990	1.74	
44-4***	2	0.83	16,500	.993	1.68	
79-10	2	0.86	17,500	1.330	2.38	
83-2	2	0.80	15,500	.950	2.29	
45-2***	3	1.15	27,300	.988	1.71	
45-4***	3	1.16	27,500	.990	1.72	
46-10***	3	0.85	17,000	1.015	1.68	
46-12***	3	0.87	17,250	.965	1.71	
83-6	3	0.80	16,000	.950	2.24	
51-2	4	0.75	14,200	.854	1.73	244% MV/A
51-4	4	0.76	14,000	.974	1.69	228% MV/A
52-2	4	0.75	14,500	.969	1.75	180% MV/A
52-4	4	0.79	15,000	.950	1.79	120% MV/A
53-2	4	0.79	15,000	.905	1.76	51% MV/A
53-4	4	0.79	15,500	.930	1.79	38% MV/A
73-10	4	**	**	.773	1.77	20% H_2 80% N_2
73-12	4	**	**	.875	1.74	20% H_2 80% N_2
80-2	4	0.72	14,000	.713	1.70	60% H_2 40% N_2
80-4	4	0.76	15,000	.549	1.67	60% H_2 40% N_2
49-2	None	0	71,000	-	1.69	
55-6	None	0	83,000	-	1.65	
55-8	None	0	83,000	-	1.72	

*Configuration 1 - Long overboard ducts and exhausterators
Configuration 2 - Short overboard ducts and exhausterators
Configuration 3 - Streamlined overboard ducts and exhausterators
Configuration 4 - Short overboard ducts only

**Instrumentation Out

***Primary Investigation Runs

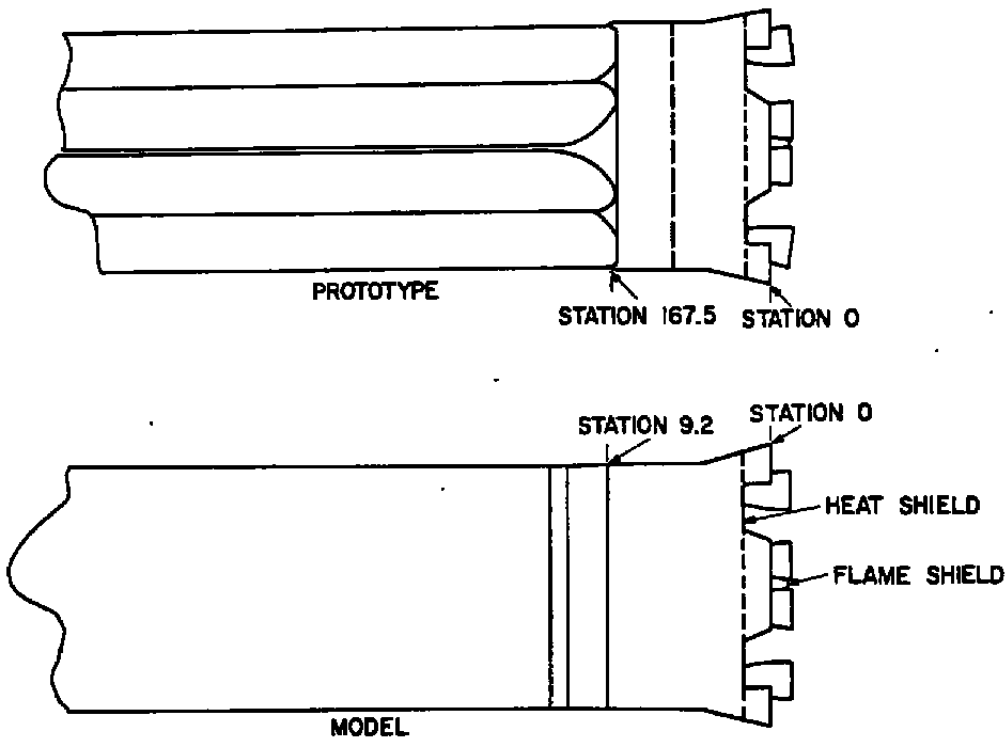

Fig. 1 Comparison of Model External Shroud Contour with Prototype

a. Three-Quarter Left View of Long Duct Configuration

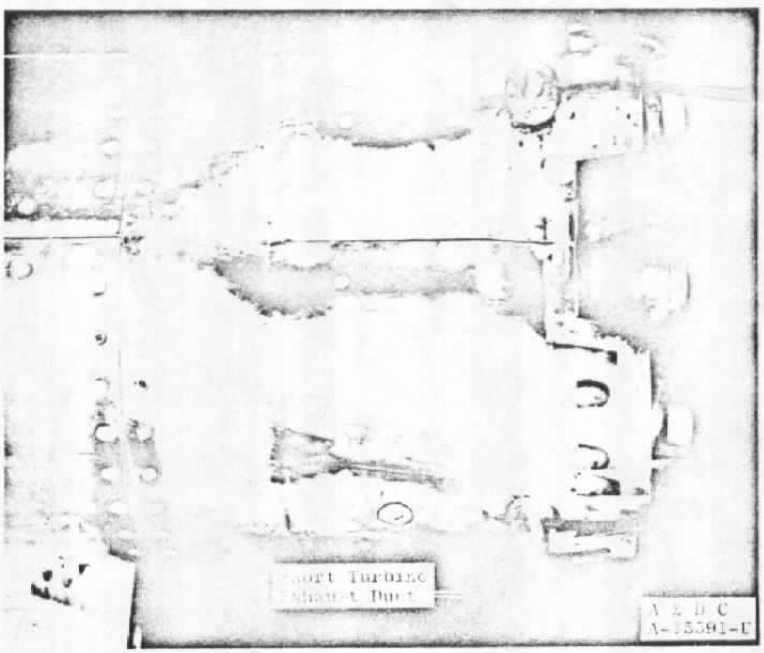

b. Side View of Short Duct Configuration

Fig. 2 Views of the 5.47-Percent Saturn Model

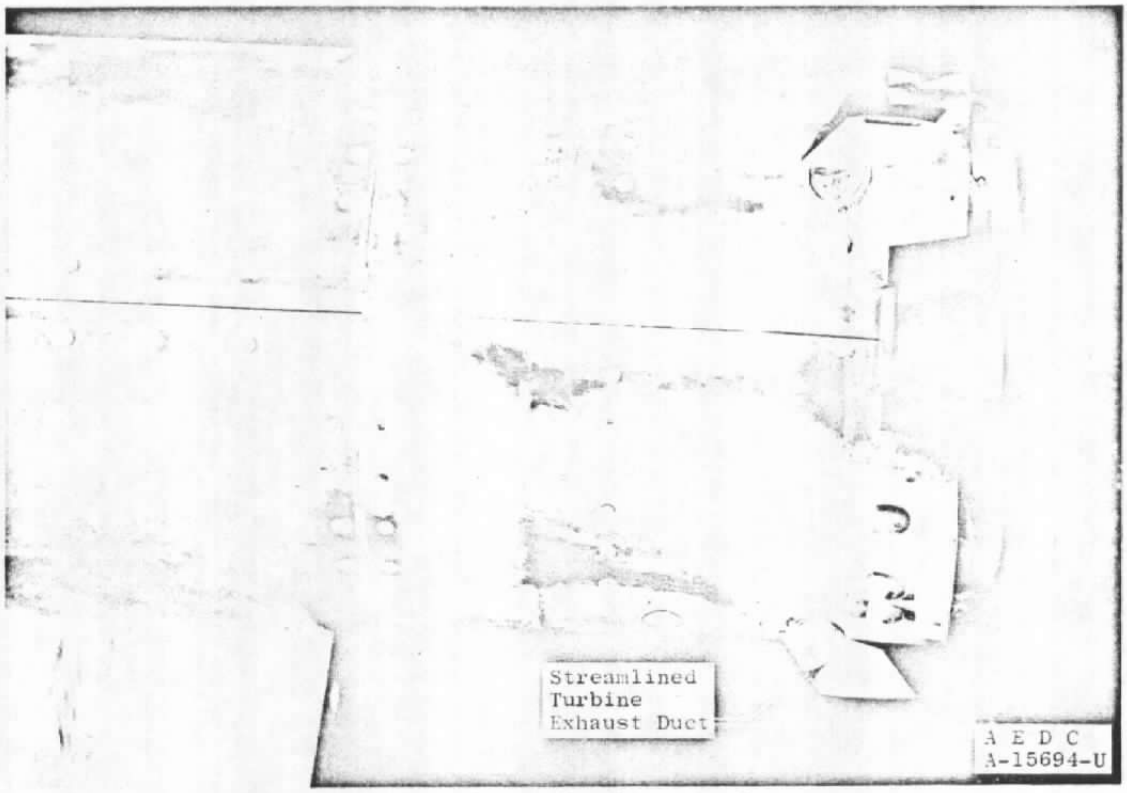

c. Side View of Streamlined Duct Configuration

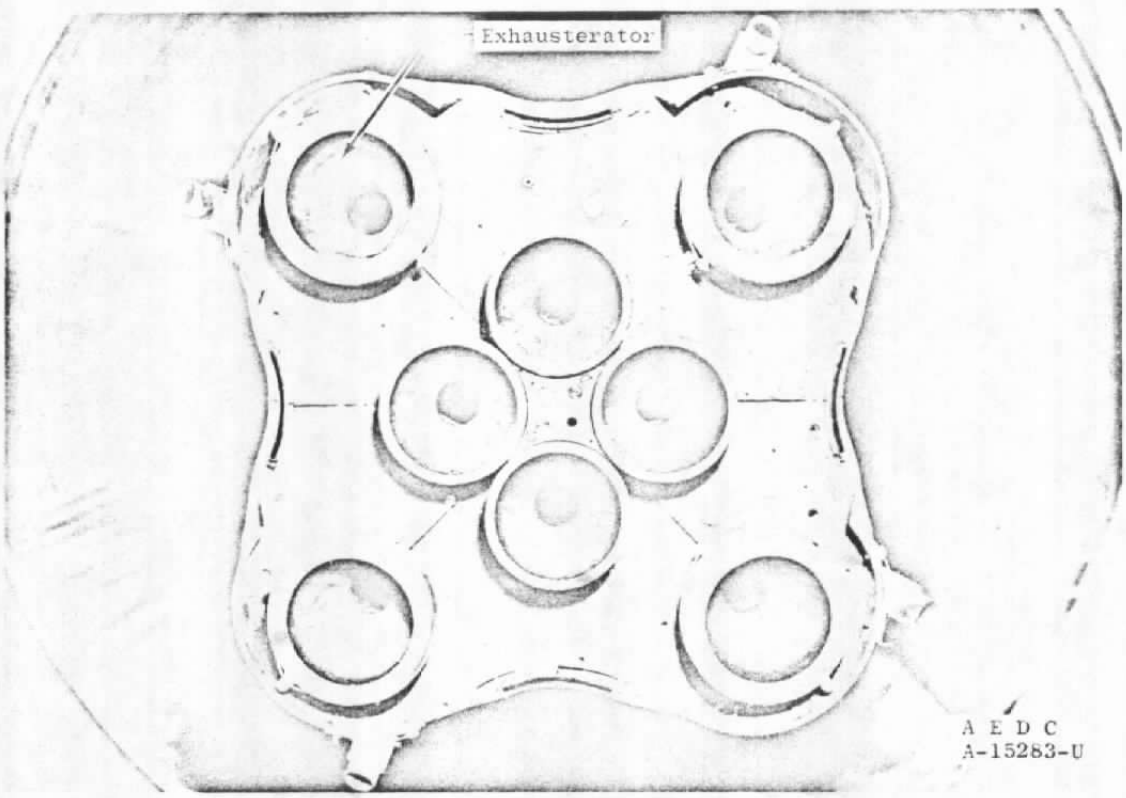

d. Rear View

Fig. 2 Concluded

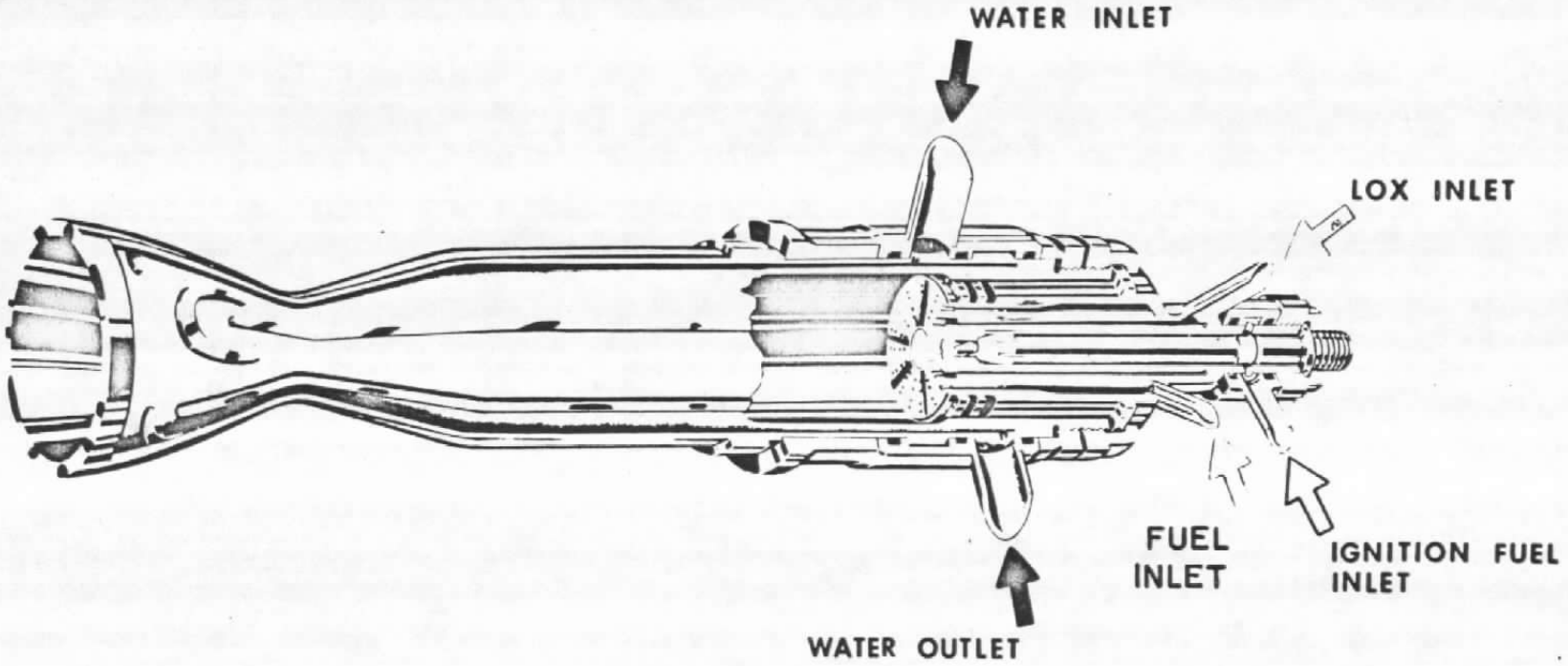

Fig. 3 Cutaway View of Model Engine

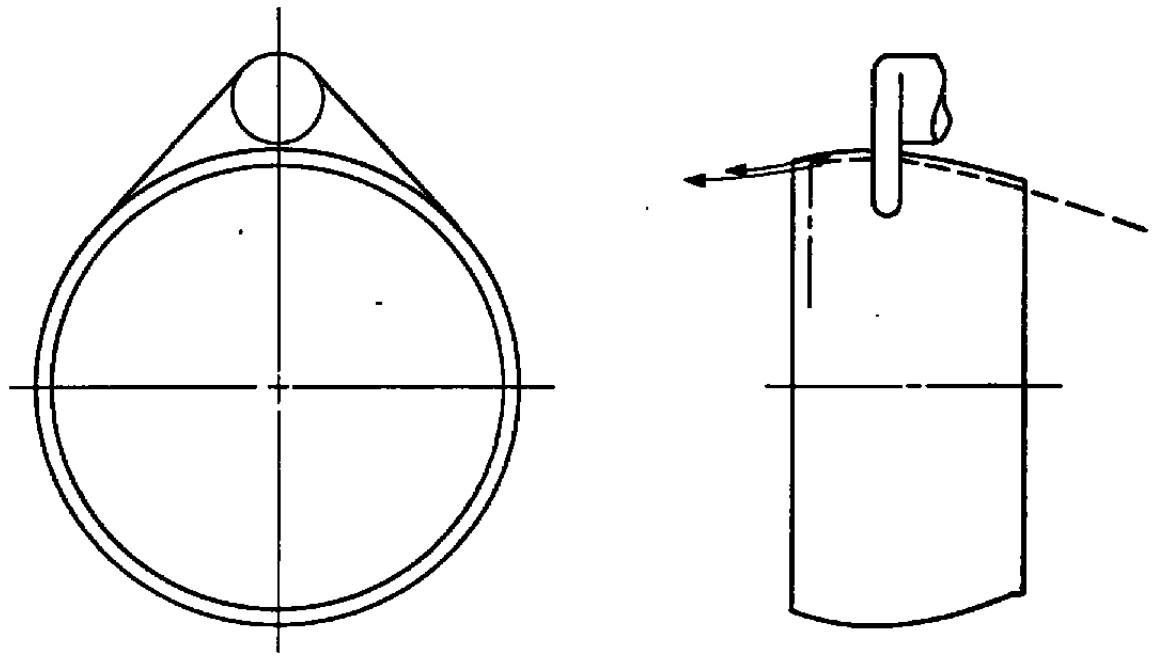

EXHAUSTERATOR FOR PROTOTYPE ENGINES

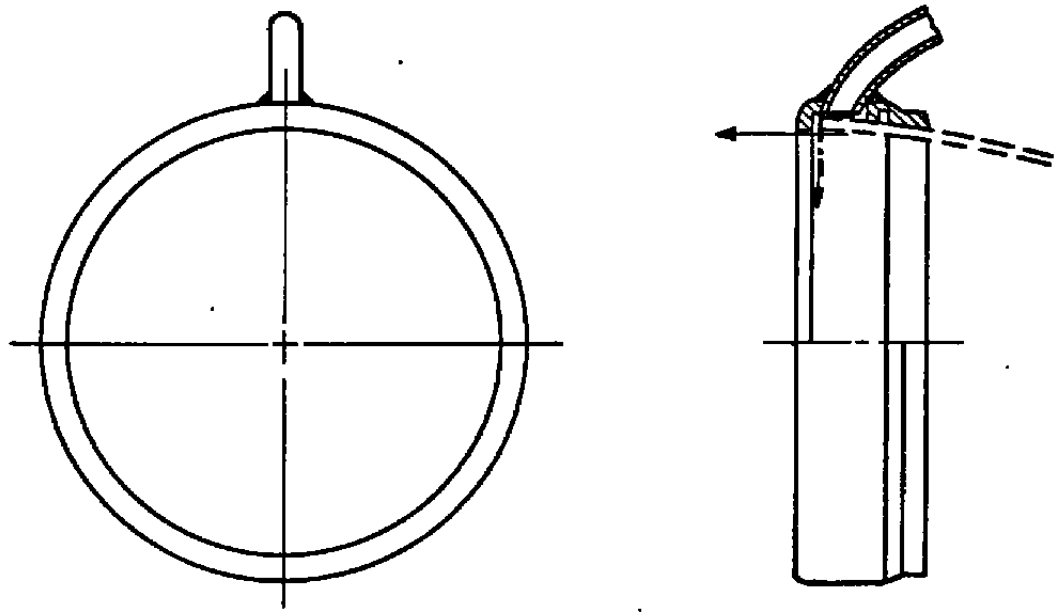

EXHAUSTERATOR FOR MODEL ENGINES

Fig. 4 Comparison of Model Exhausterator Design with Prototype

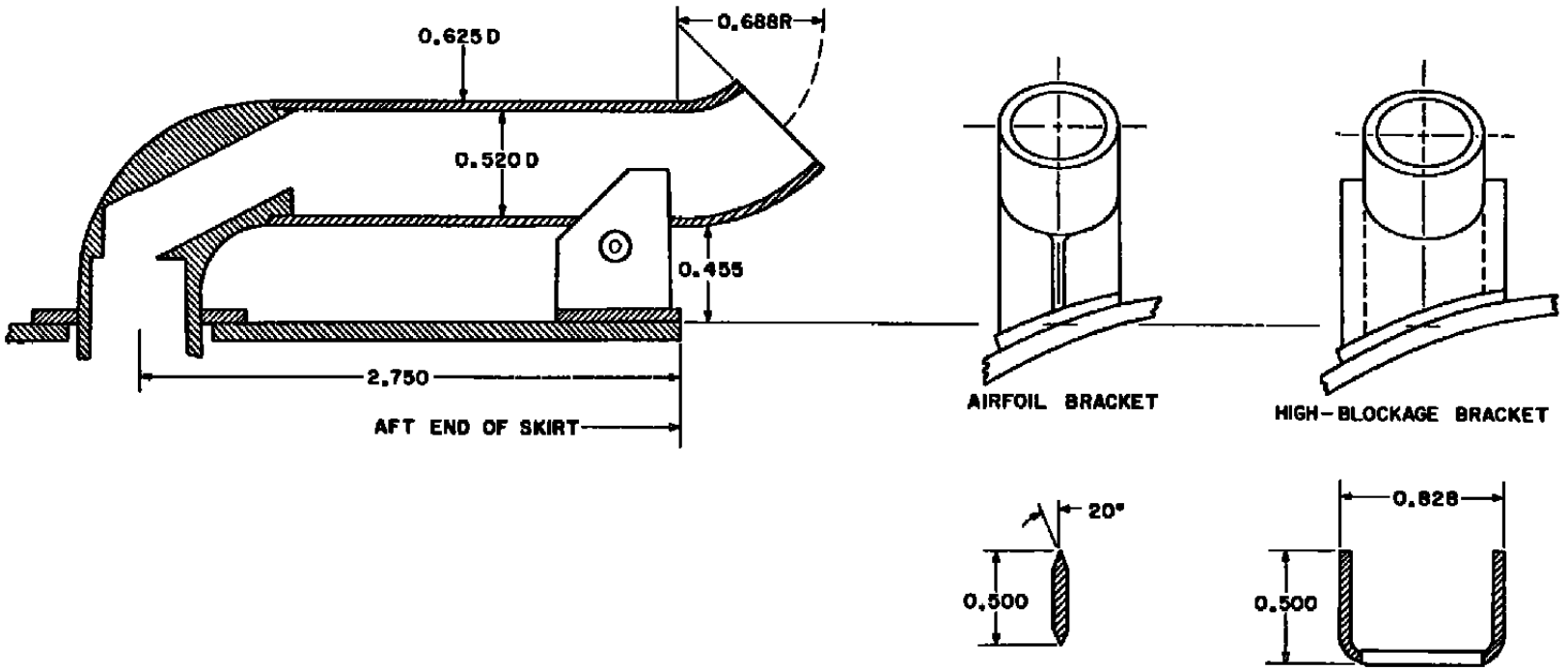

a. Long Duct Configuration

Fig. 5 Details of Model Overboard Turbine Exhaust Duct Configuration

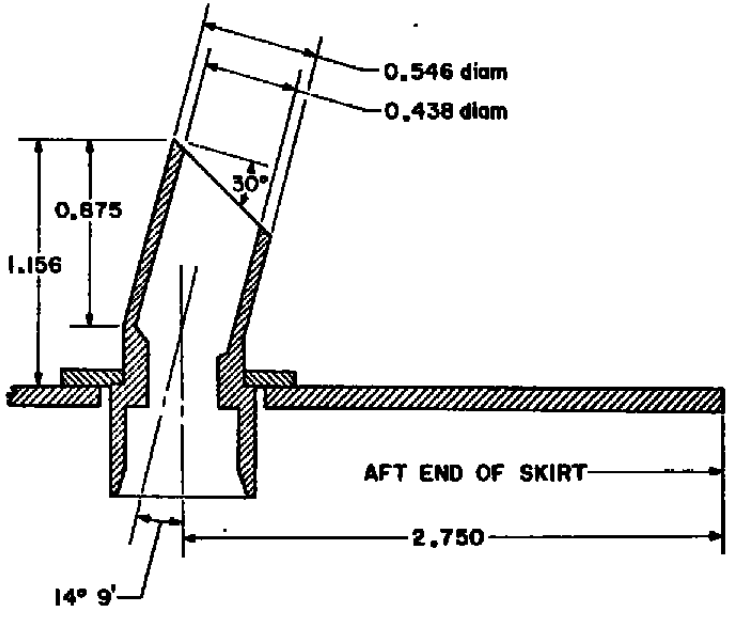

b. Short Duct Configuration

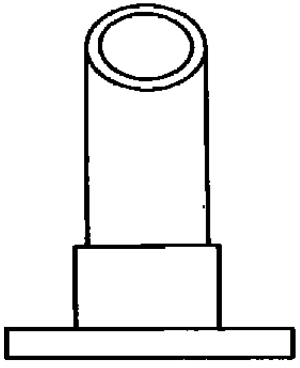

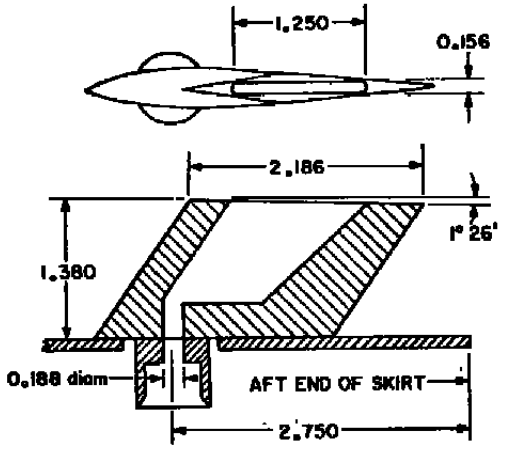

c. Streamlined Duct Configuration

Fig. 5 Concluded

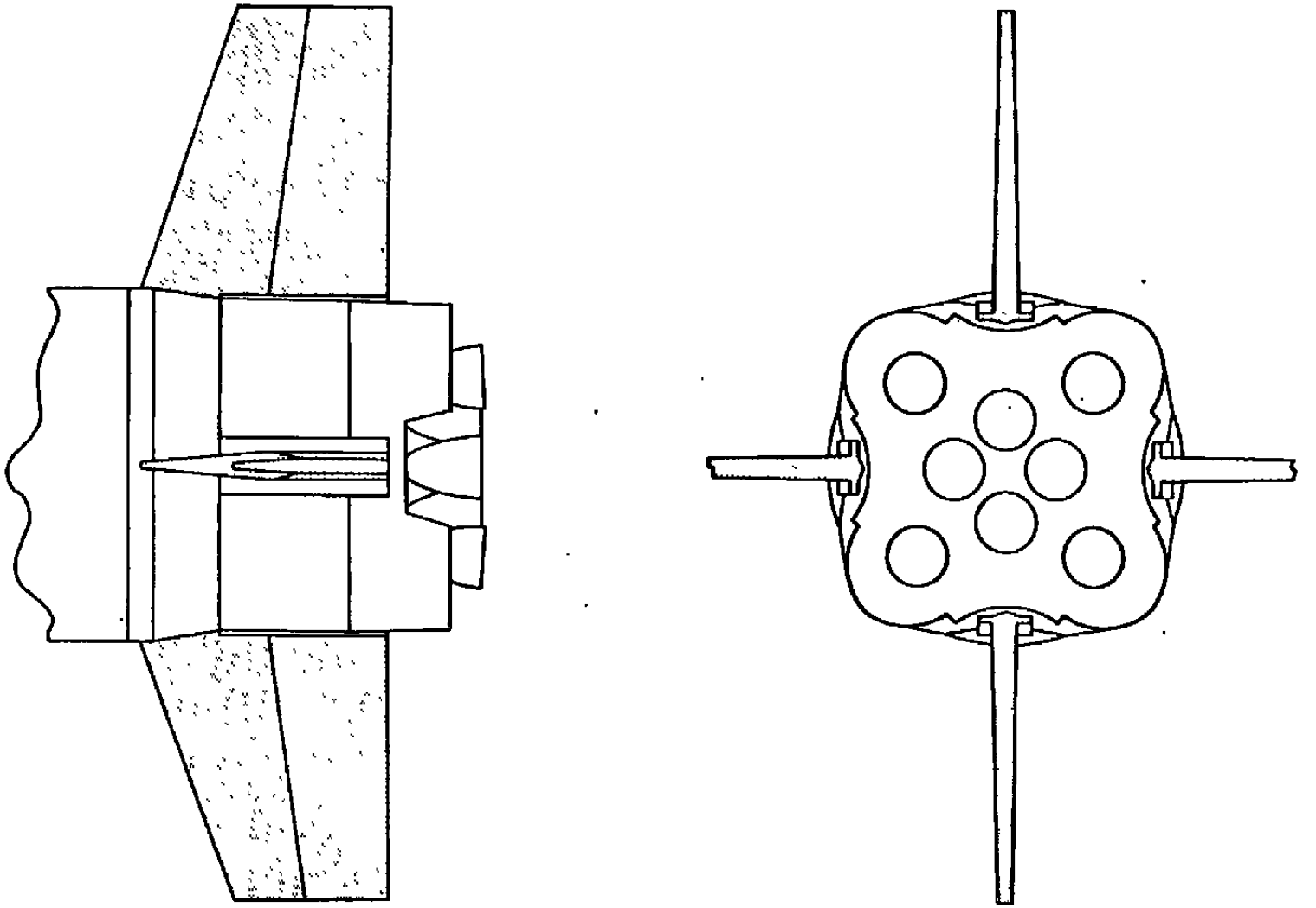

Fig. 6 Location of Model Stabilizing Fins

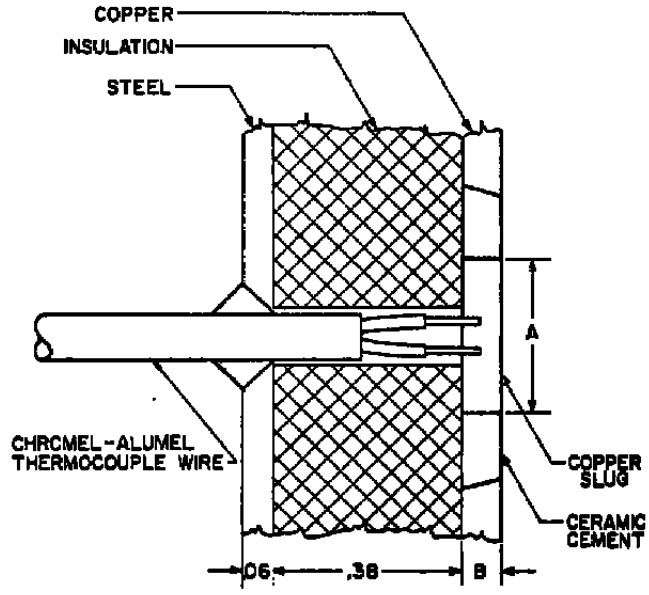

	HEAT SHIELD	FLAME SHIELD
A	.4375	.3170
B	.065	.125
NOMINAL WEIGHT-GMS	1.397	.987

Fig. 7 Details of Heat and Flame Shield Calorimeters

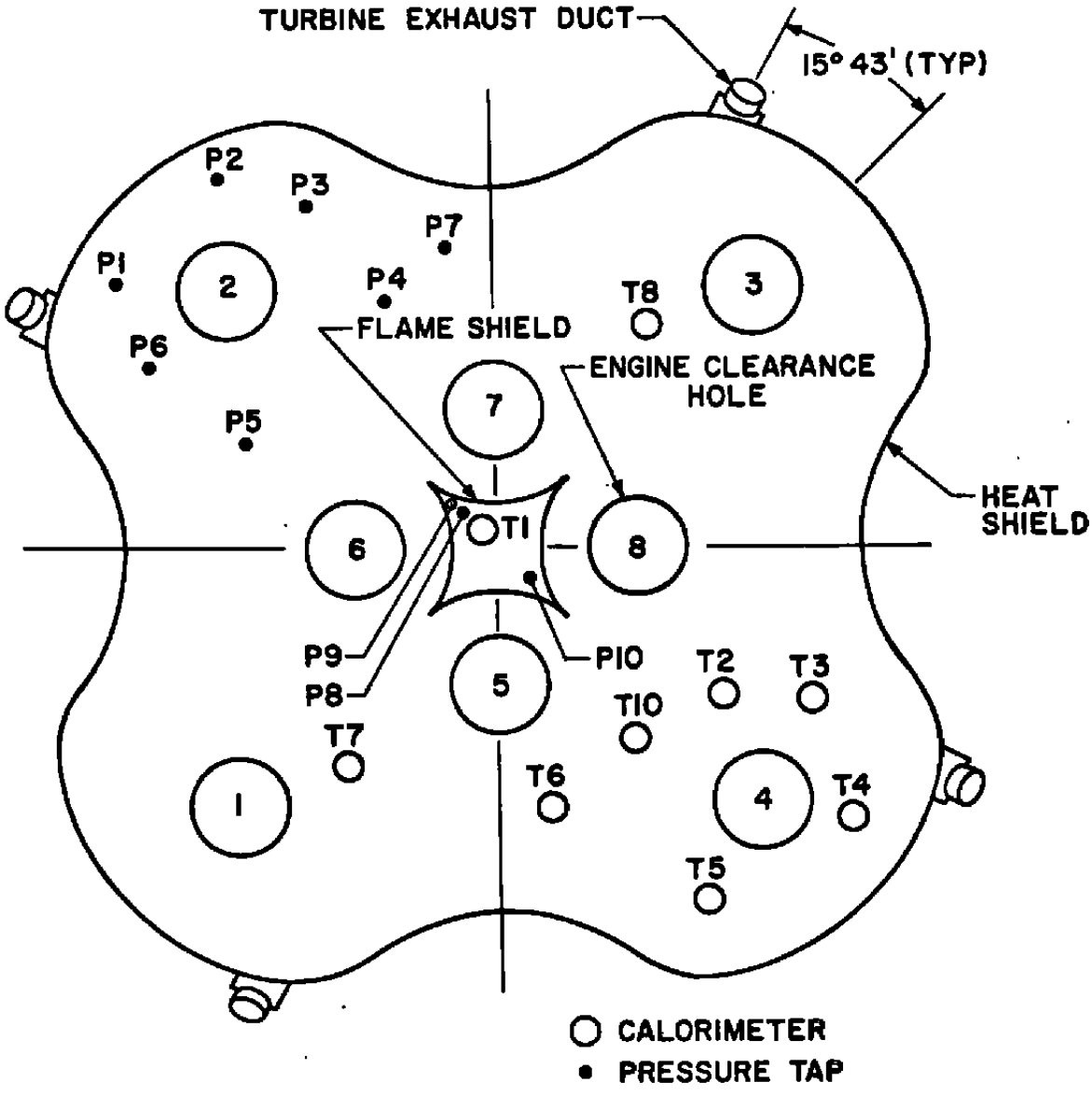

Fig. 8 Location of Heat and Flame Shield Instrumentation

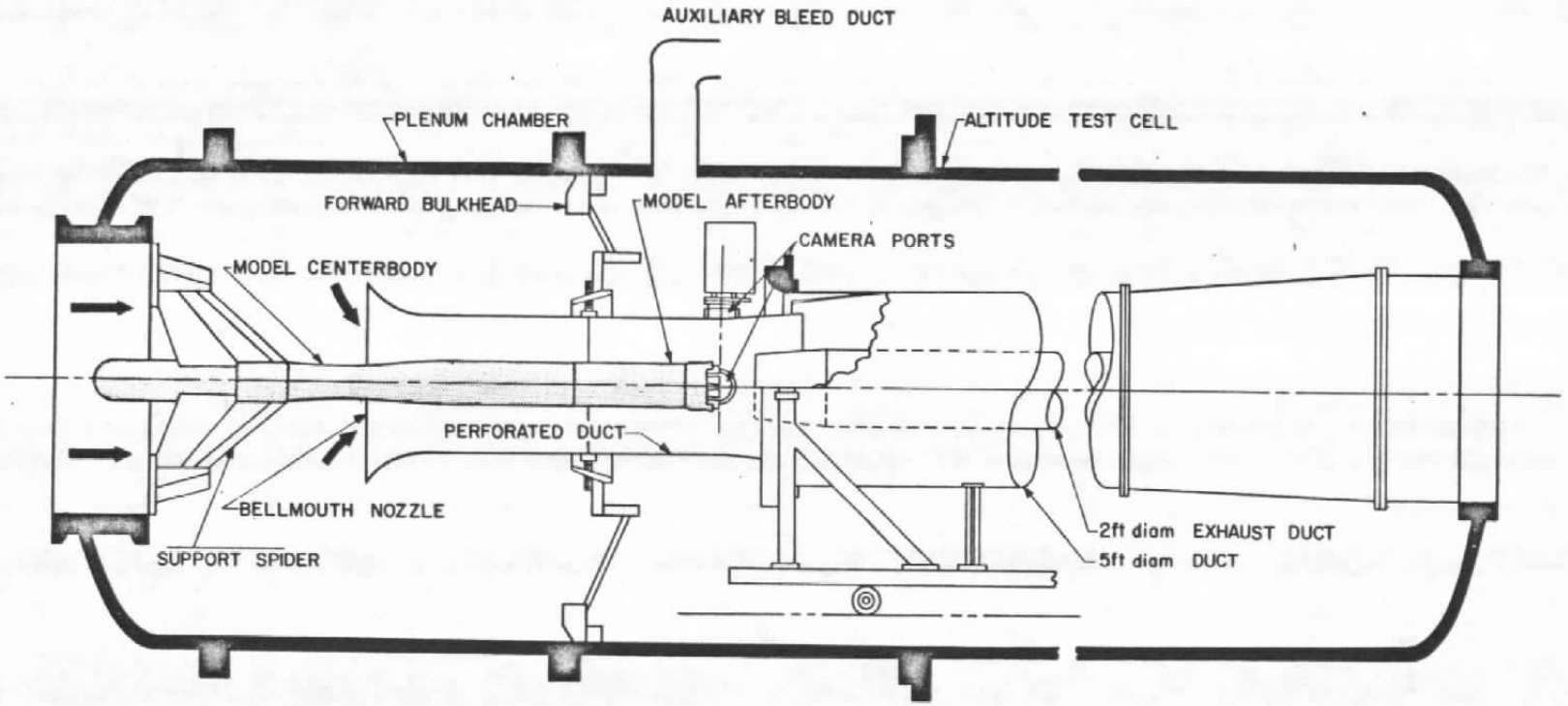

Fig. 9 Schematic of Model Installation in Rocket Altitude Cell T-1

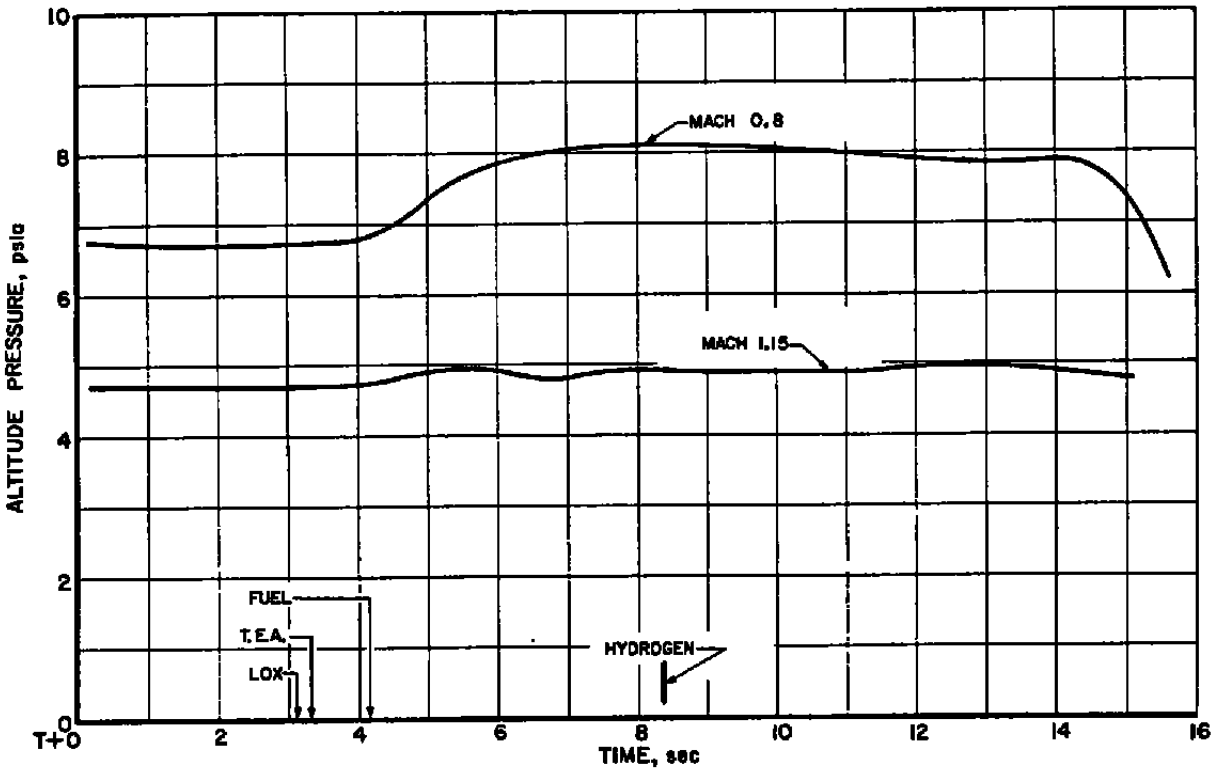

a. Test Section Altitude Pressure

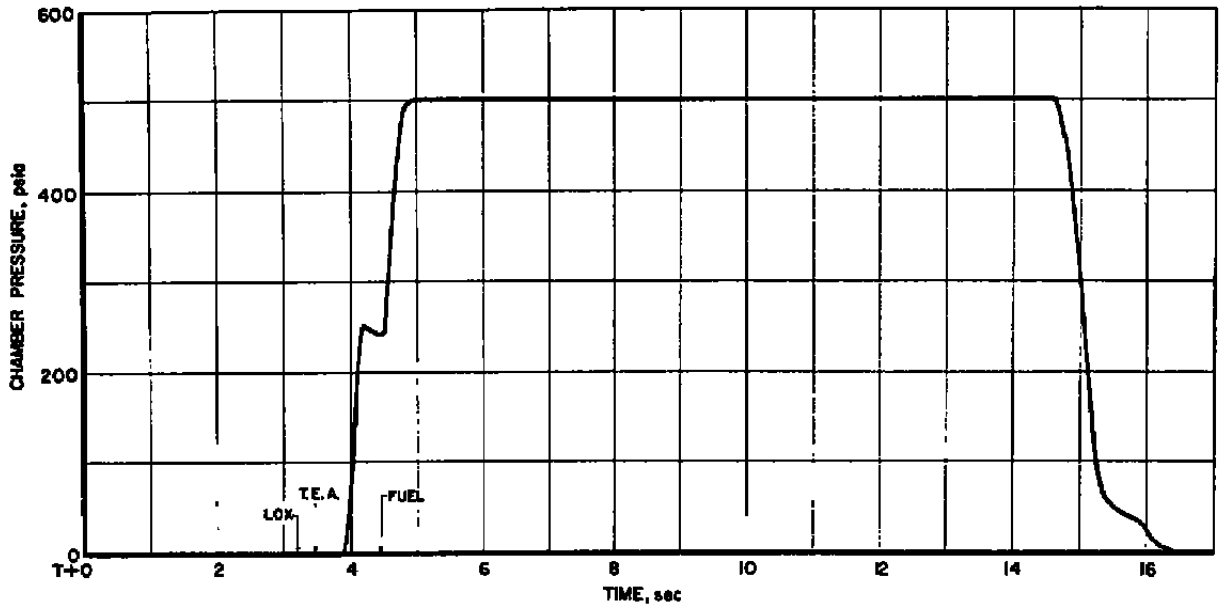

b. Engine Chamber Pressure

Fig. 10 Typical Test Cell and Engine Chamber Pressure-Time Histories

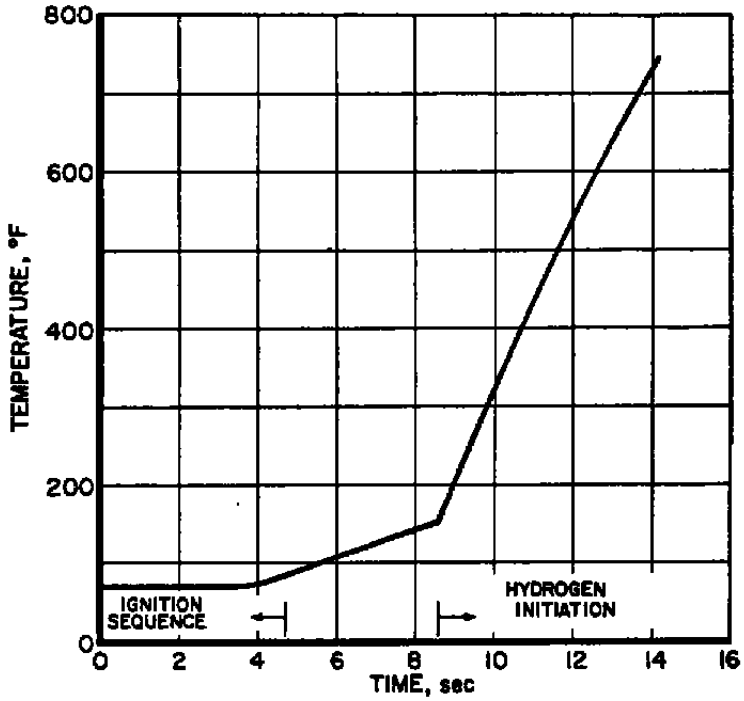

a. Temperature

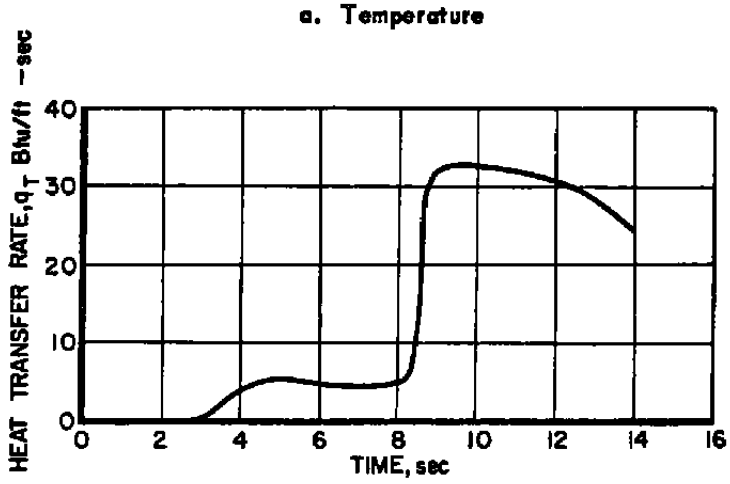

b. Heat Transfer

Fig. 11 Typical Base Calorimeter Temperature and Heat Transfer-Time Histories

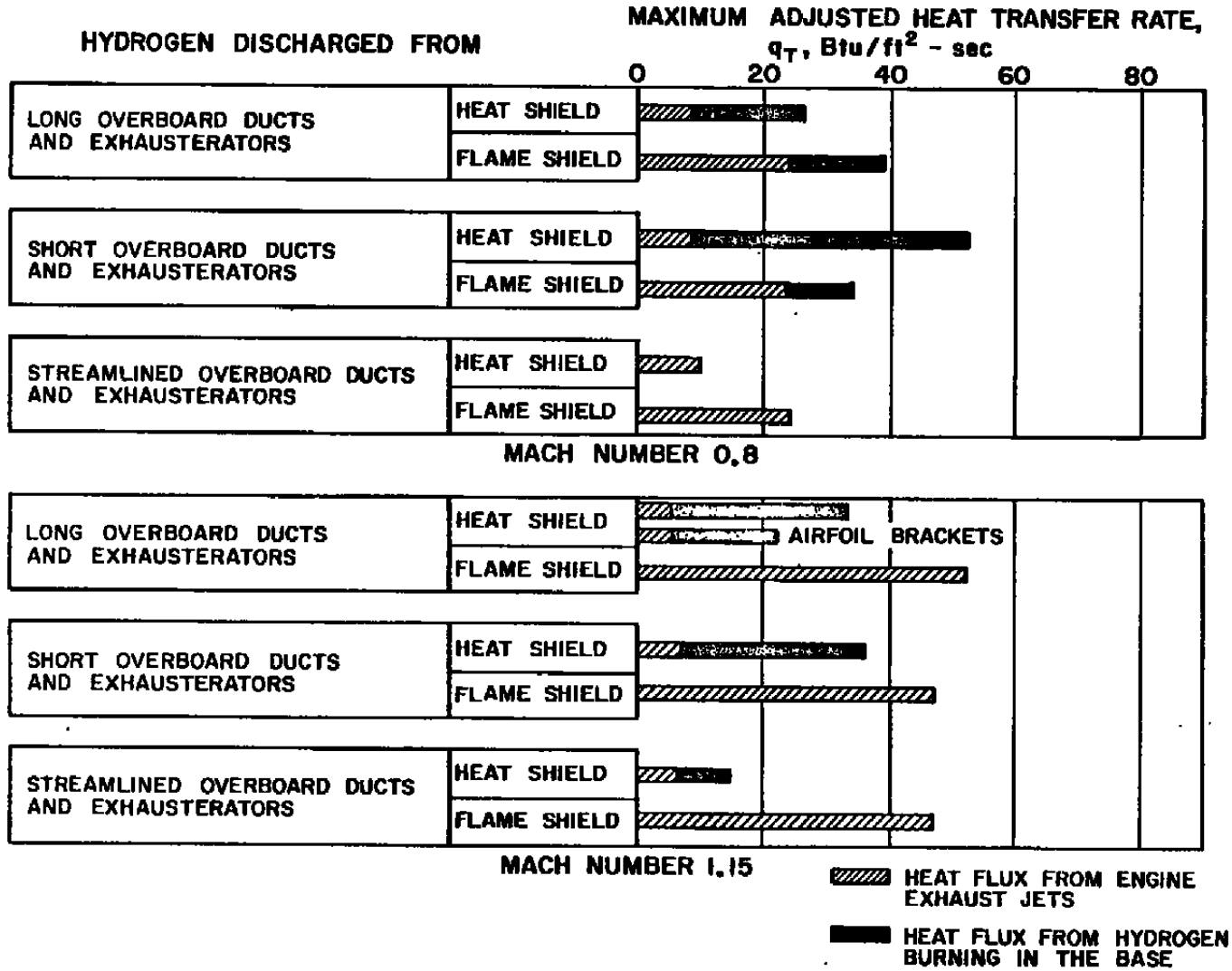

Fig. 12 Comparison of Maximum Total Heat Transfer Rates for Three Overboard Turbine Exhaust Duct Configurations at Mach Numbers 0.8 and 1.15

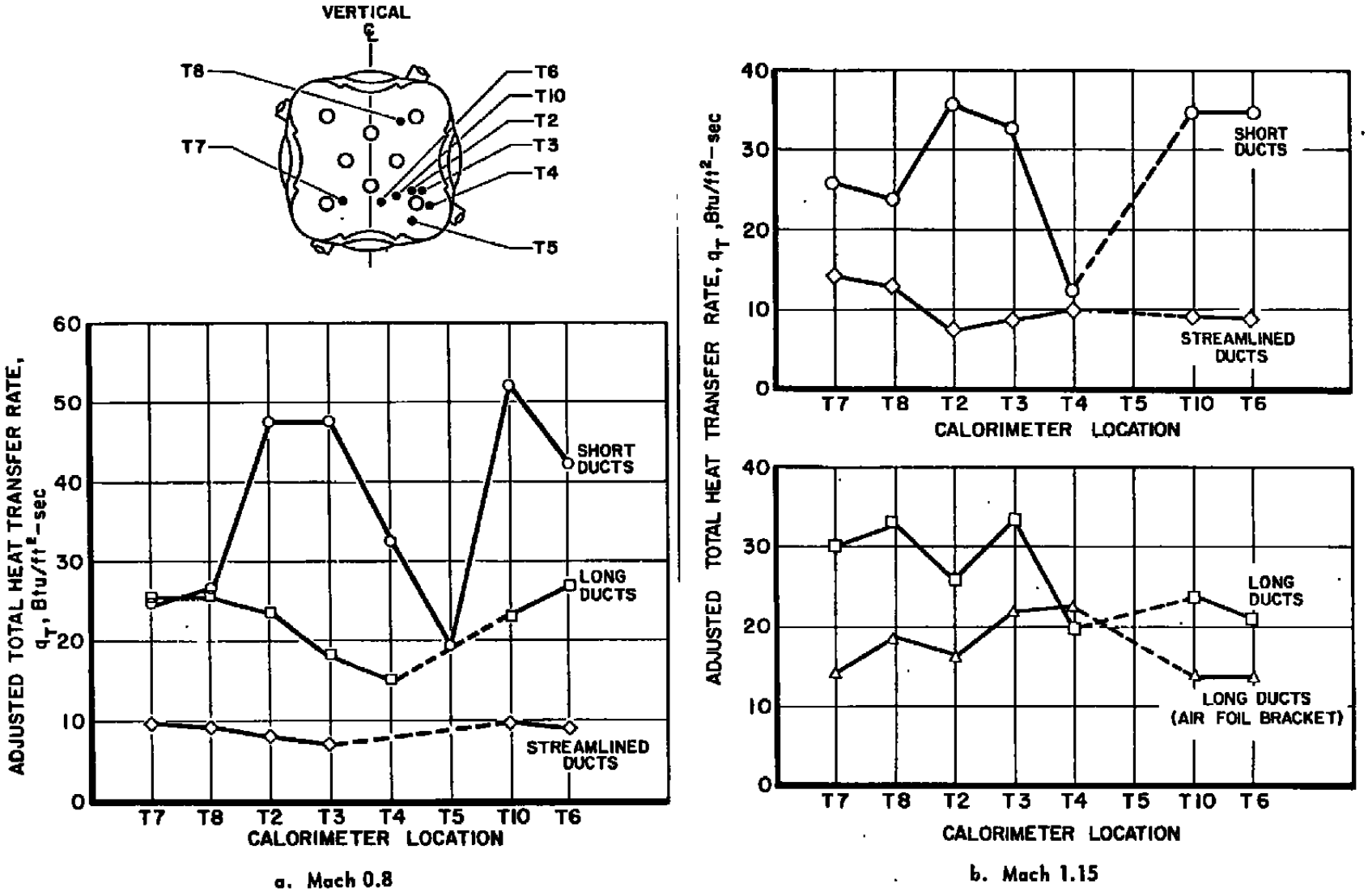

Fig. 13 Distribution of Total Heat Transfer Rates over Model Base

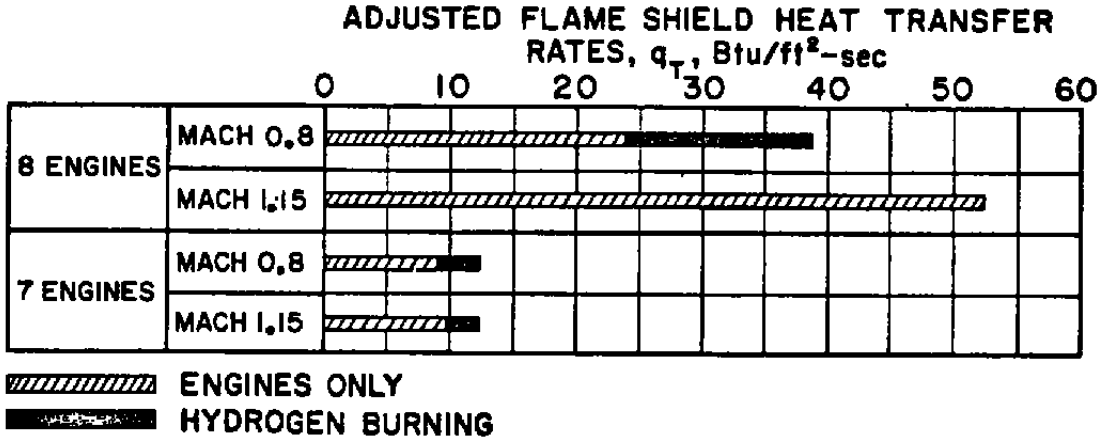

a. Flame Shield

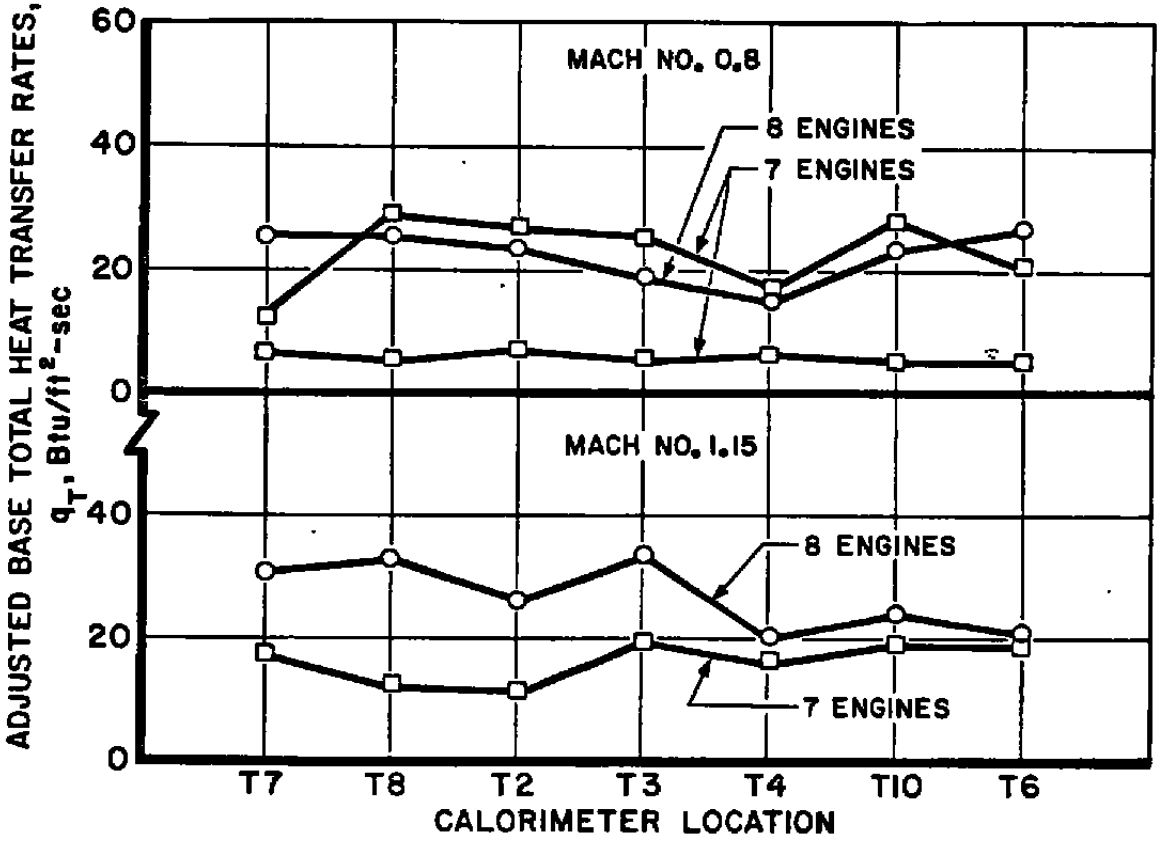

b. Heat Shield

Fig. 14 Comparison of Total Heat Transfer Rates for Seven and Eight-Engine Operation

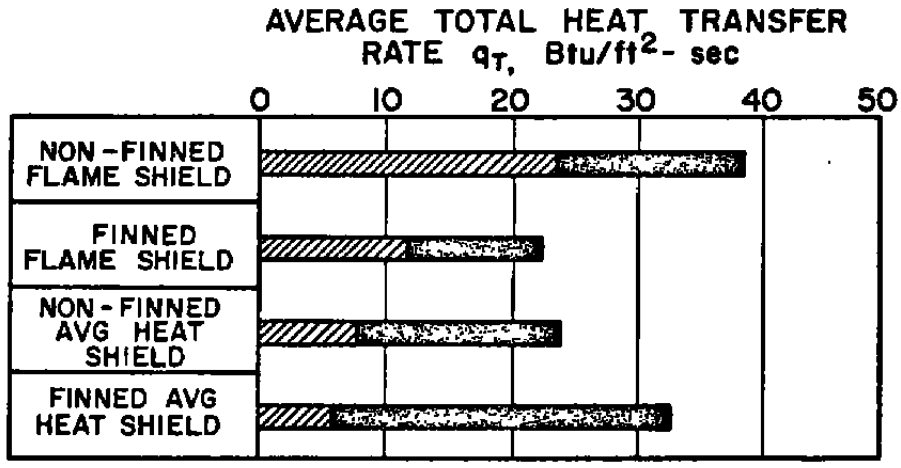

a. Average Heating Rates

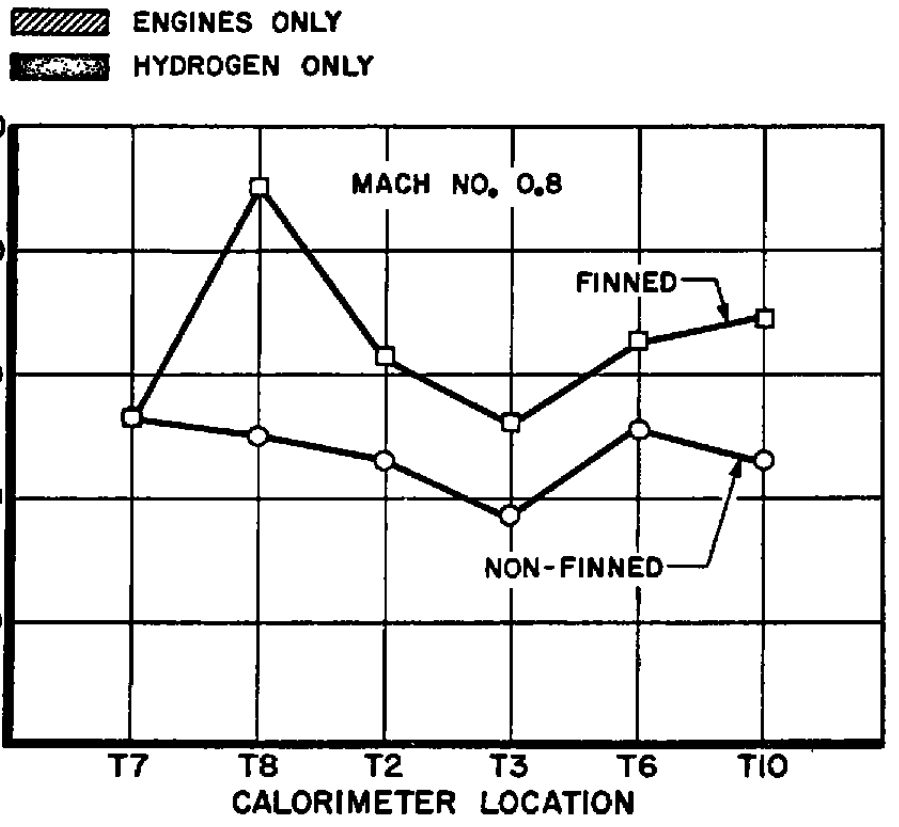

b. Heating Rate Distribution on Model Base

Fig. 15 Comparison of Total Heat Transfer Rates with and without Stabilizing Fins

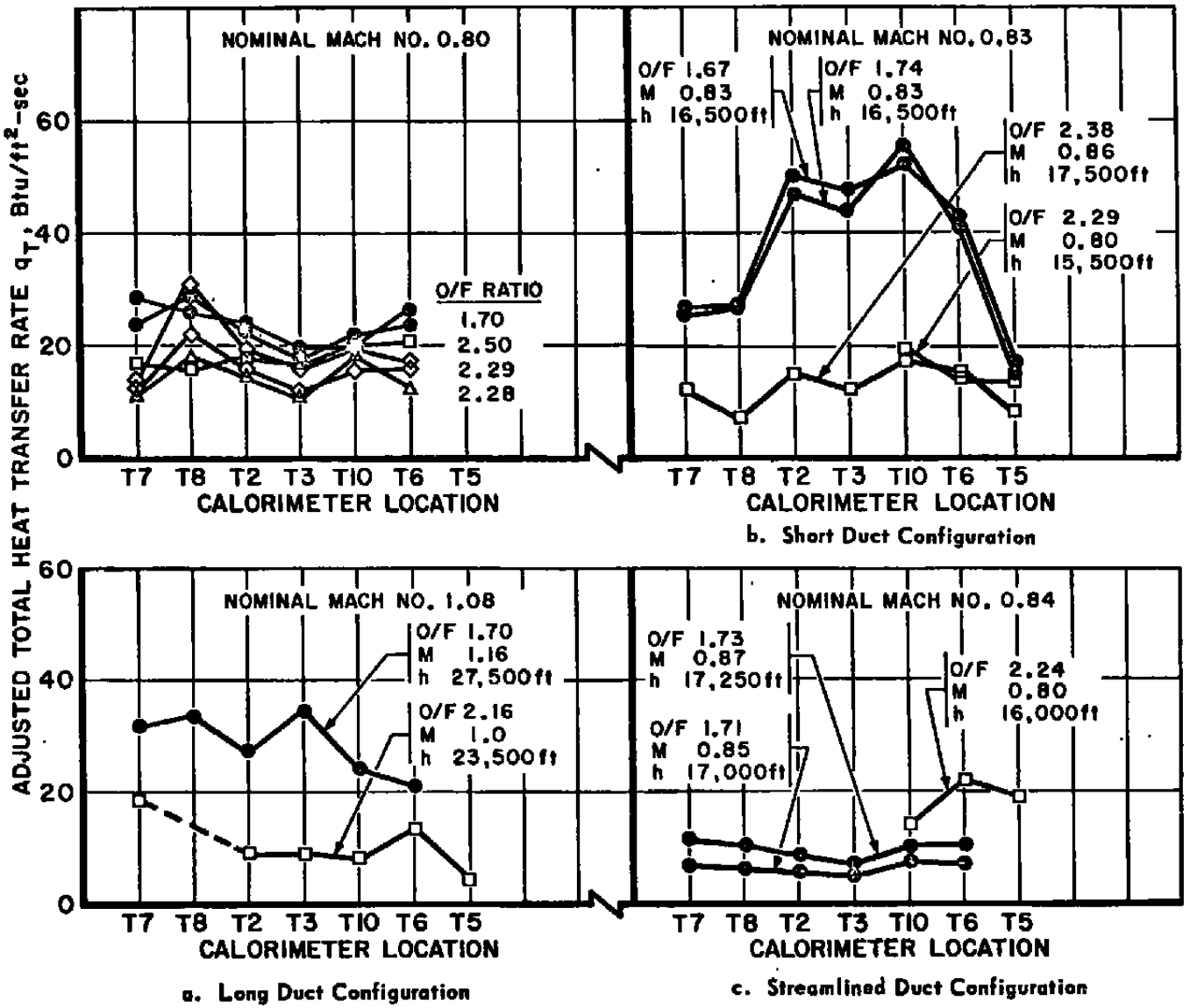

b. Short Duct Configuration

a. Long Duct Configuration

c. Streamlined Duct Configuration

Fig. 16 Effect of O/F Ratio on Base Heating

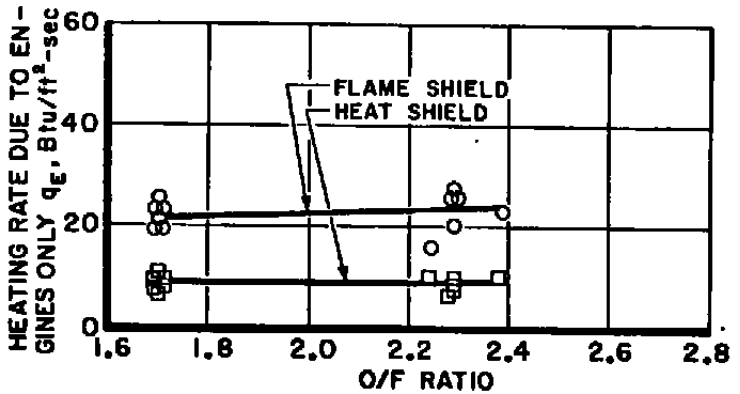

d. Heating Rates Caused by Engine Exhaust Only

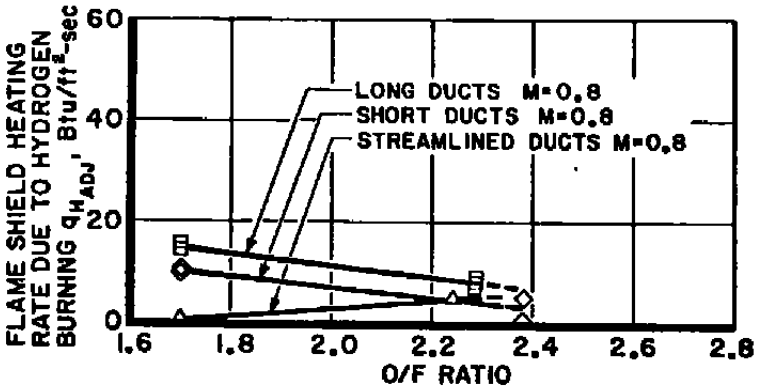

e. Increase in Flame Shield Heating Rate Caused by Hydrogen Burning

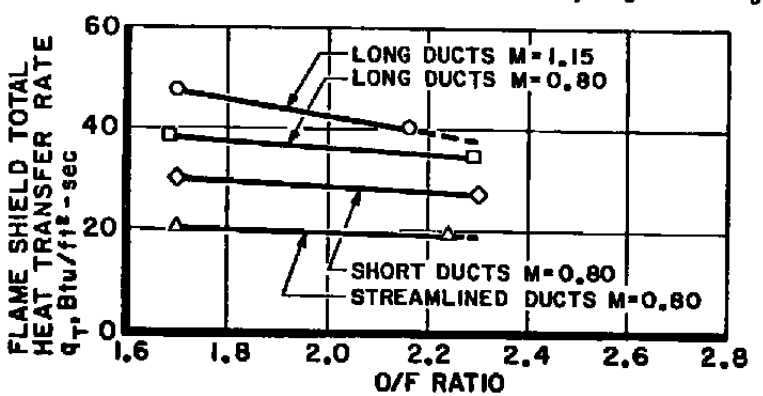

f. Flame Shield Total Heat Transfer Rates

Fig. 16 Concluded

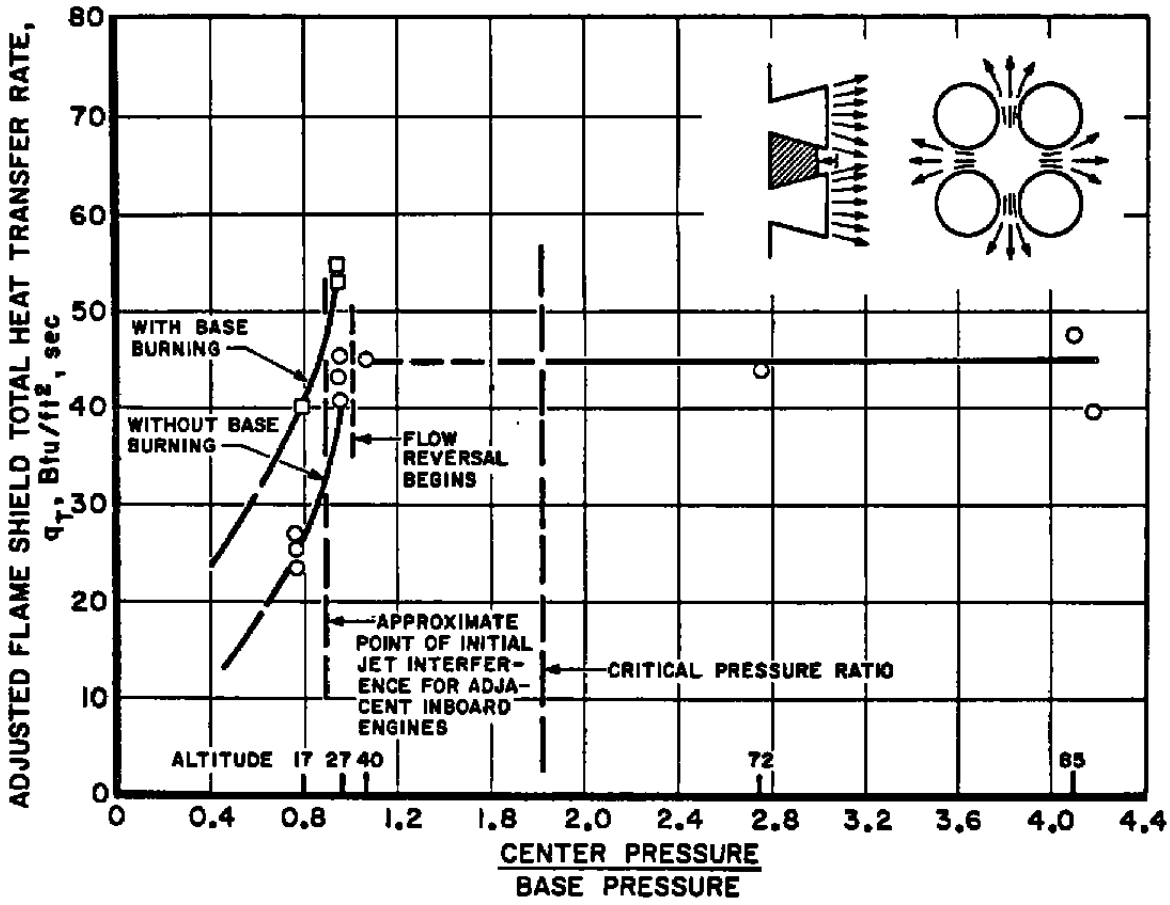

Fig. 17 Variation of Flame Shield Total Heat Transfer Rate with Altitude

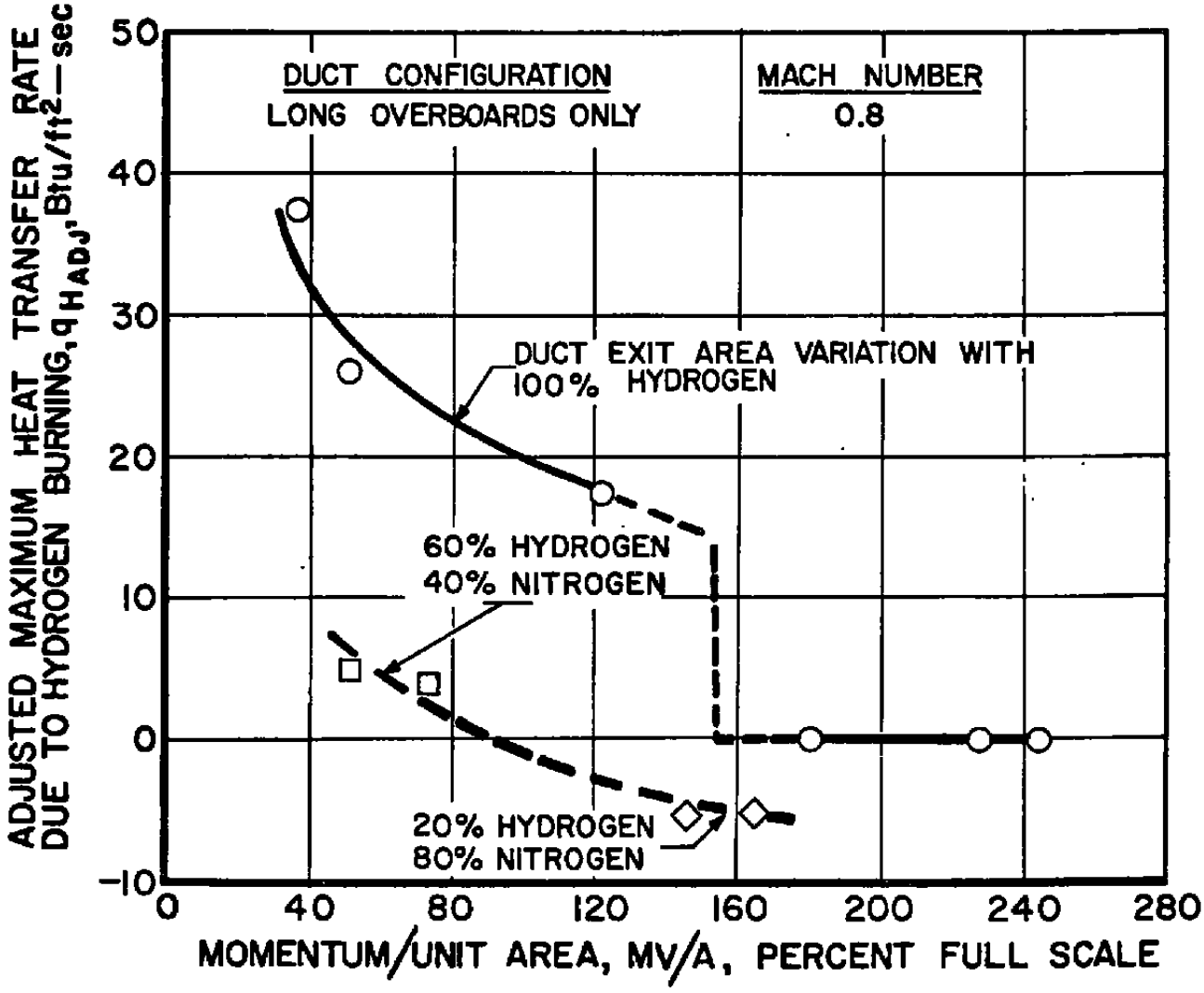

Fig. 18 Effect of Turbine Exhaust Gas Momentum on Base Heating

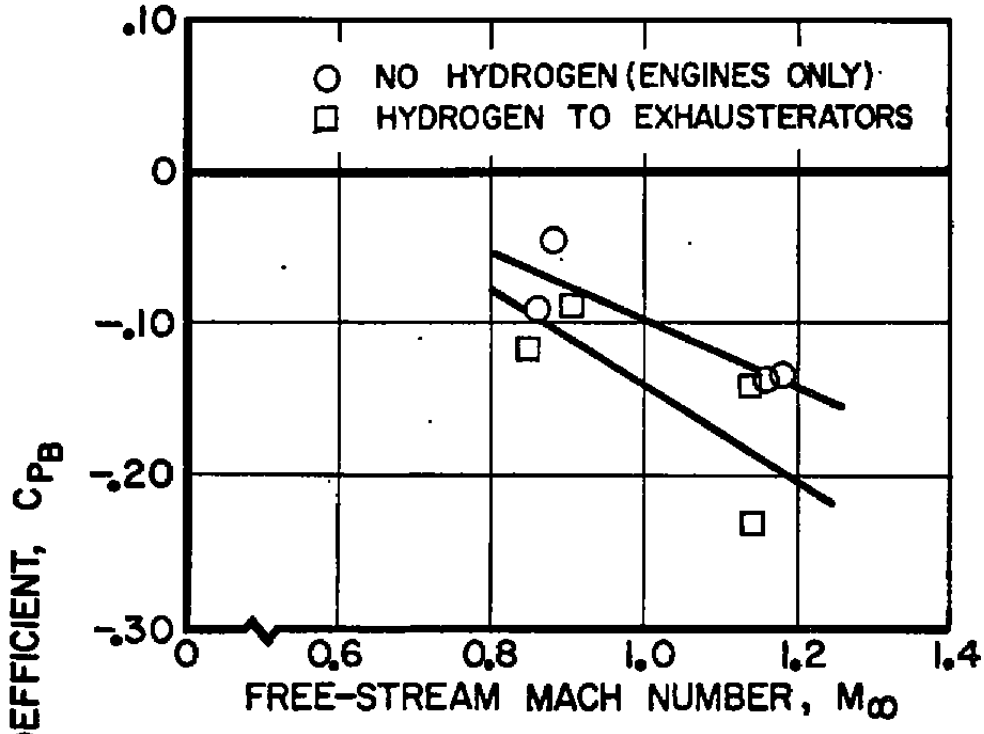

a. No Base Burning

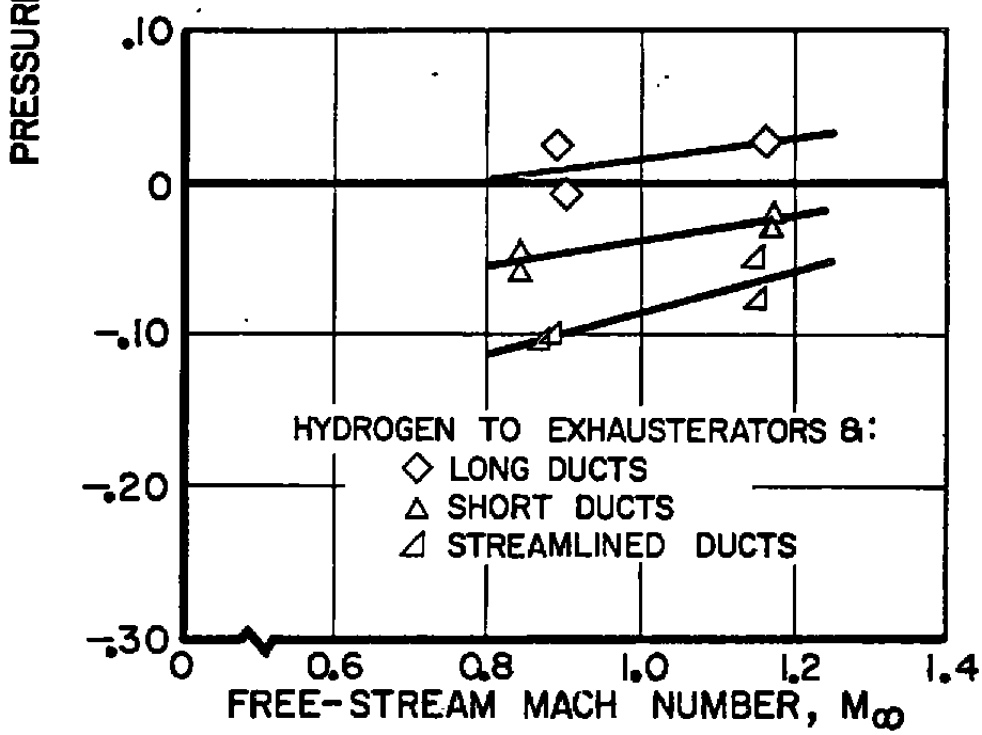

b. Base Burning

Fig. 19 Variation of Base Pressure Coefficient with Free-Stream Mach Number

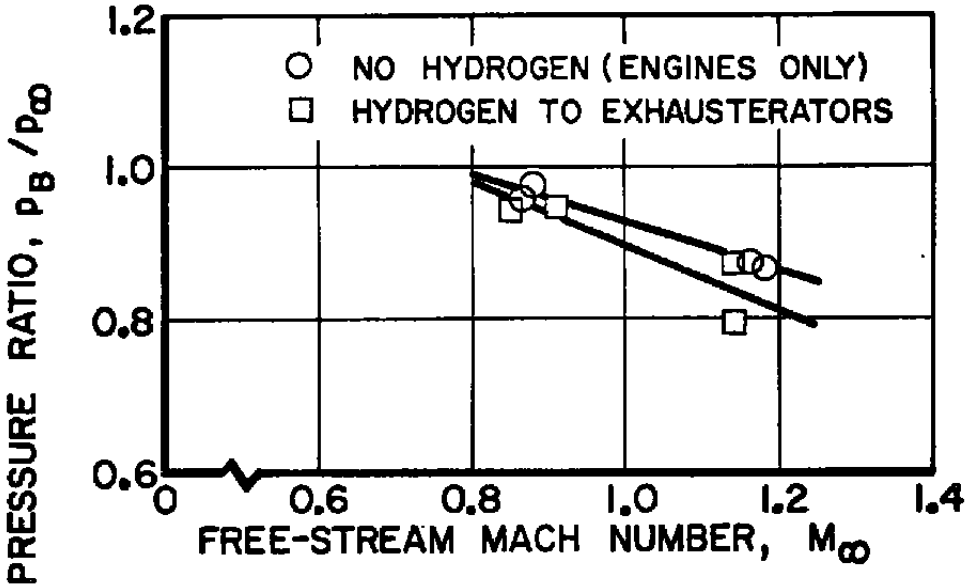

a. No Base Burning

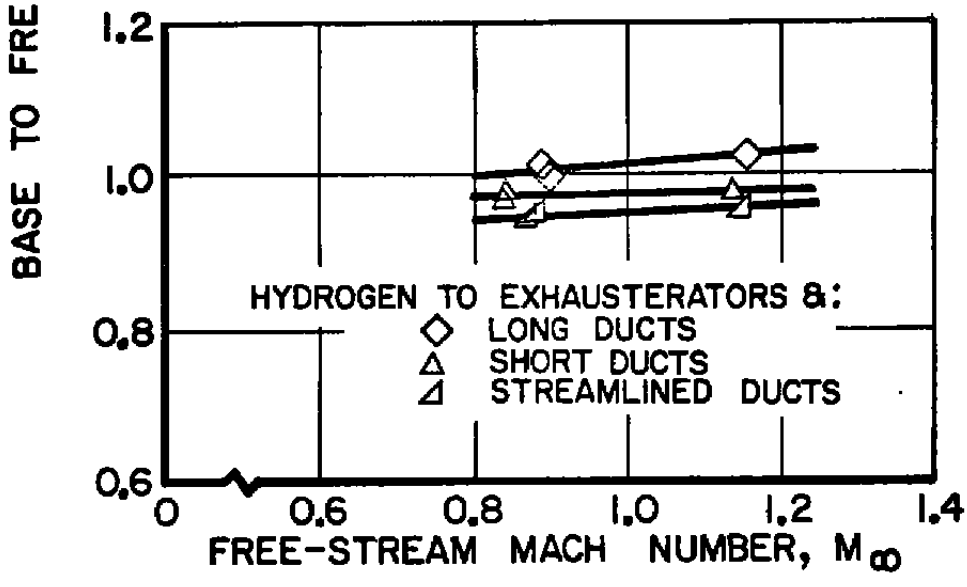

b. Base Burning

Fig. 20 Variation of Base to Free-Stream Pressure Ratio with Free-Stream Mach Number

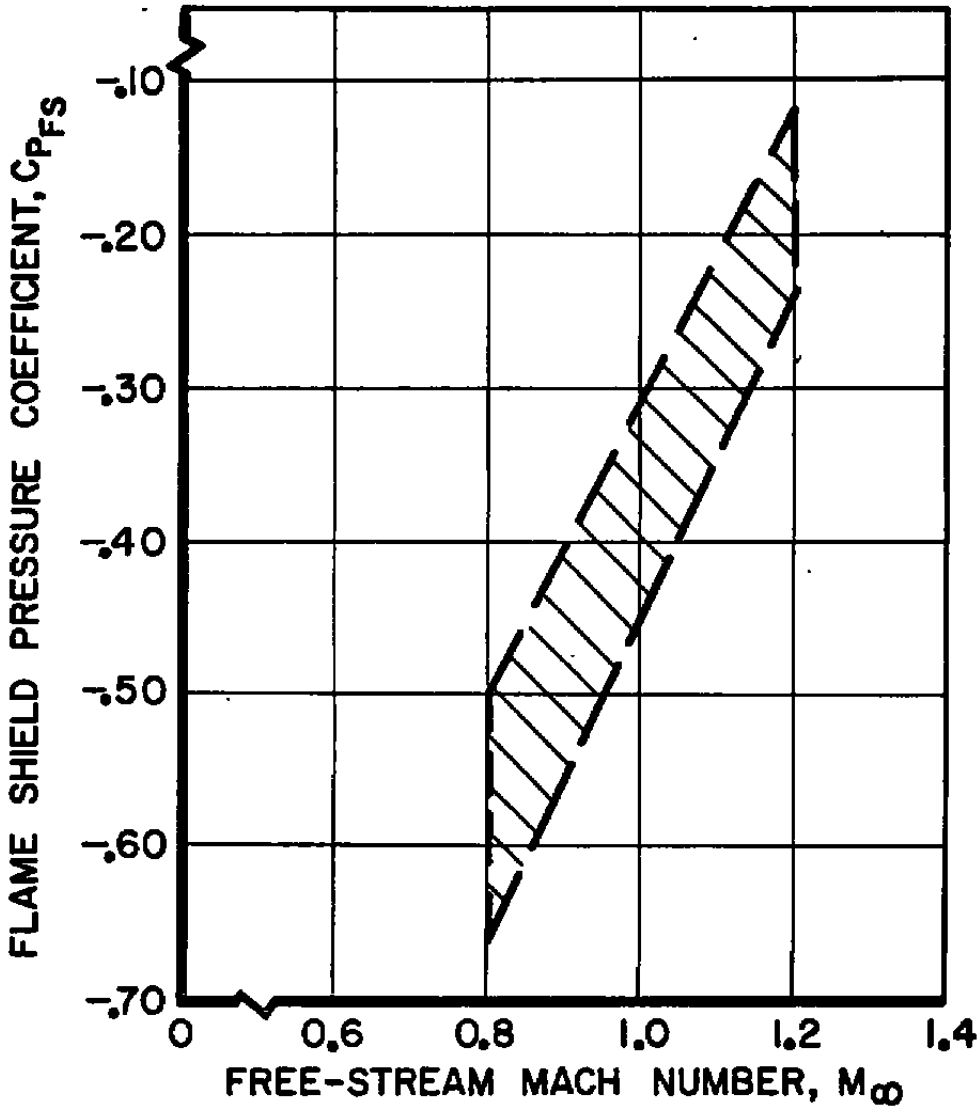

a. Pressure Coefficient

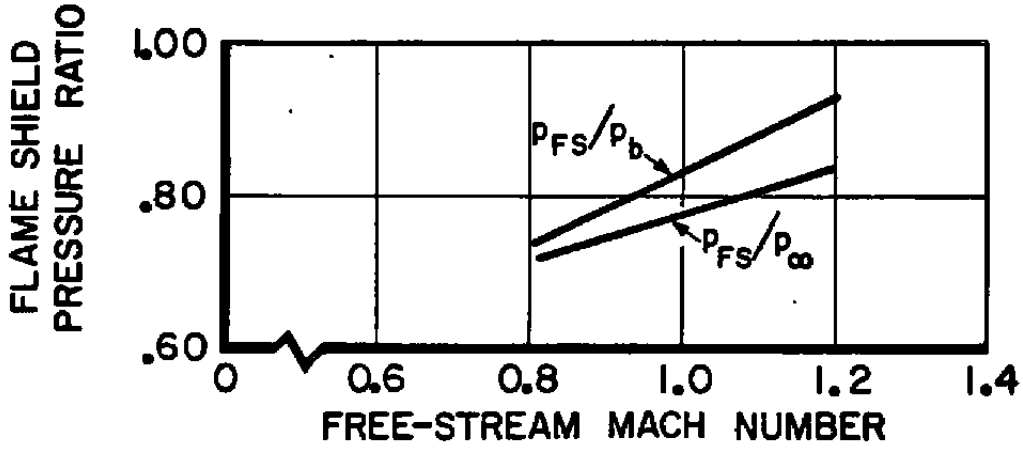

b. Pressure Ratio

Fig. 21 Variation of Flame Shield Pressure Coefficient and Pressure Ratio with Free-Stream Mach Number

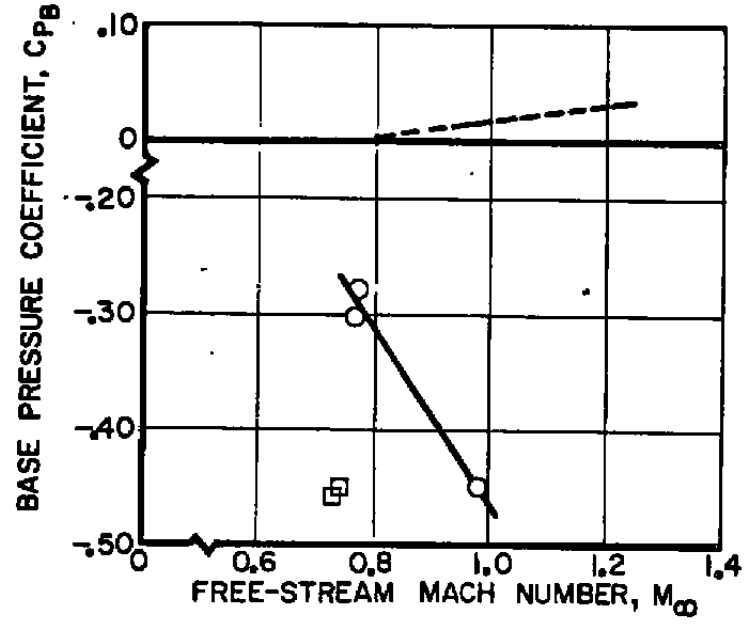

a. Pressure Coefficient

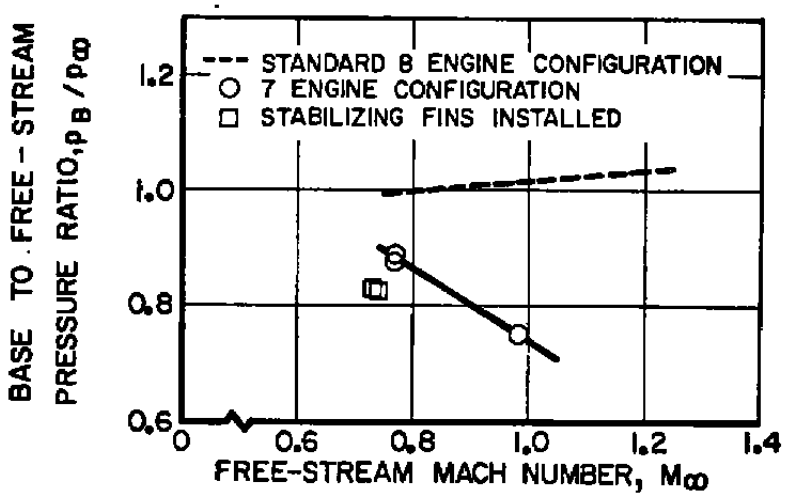

b. Pressure Ratio

Fig. 22 Variation of Base to Free-Stream Pressure Ratio and Base Pressure Coefficient with Free-Stream Mach Number for Seven-Engine and Finned-Model Configurations